A sensitive and versatile cell-based assay combines luminescence and trapping approaches to monitor unconventional protein secretion

Morgane Denus, Aurore Filaquier, William Fargues, Eloïse Néel, Sarah E Stewart, Maëlle Colladant, Thomas Curel, Alexandre Mezghrani, Philippe Marin, Sylvie Claeysen, et al.

A sensitive and versatile cell-based assay combines luminescence and trapping approaches to monitor unconventional protein secretion

Morgane Denus [1, &], Aurore Filaquier [1, &], William Fargues [1, &], Eloïse Néel [1], Sarah E. Stewart [2], Maëlle Colladant [1], Thomas Curel [1], Alexandre Mezghrani [3], Philippe Marin [1], Sylvie Claeysen [1], David C. Rubinsztein [4, 5], Marie-Laure Parmentier [1, §, #], Julien Villeneuve [1, §, #]

(1) Institute of Functional Genomics (IGF), University of Montpellier, CNRS, INSERM, Montpellier, France.

(2) Department of Biochemistry and Chemistry, School of Agriculture, Biomedicine and Environment, La Trobe Institute for Molecular Science, La Trobe University, Melbourne, VIC 3086, Australia.

(3) Centre de Biologie Structurale (CBS), University of Montpellier, CNRS, INSERM, Montpellier, France.

(4) Department of Medical Genetics, University of Cambridge, Cambridge Institute for Medical Research, The Keith Peters Building, Cambridge Biomedical Campus, Hills Road, Cambridge, CB2 0XY, United Kingdom.

(5) UK Dementia Research Institute, The Keith Peters Building, Cambridge Biomedical Campus, Hills Road, Cambridge, CB2 0XY, United Kingdom.

(&) Joint first authors

(§) Joint last authors

(#) Correspondence to Marie-Laure Parmentier (marie-laure.parmentier@igf.cnrs.fr) and to Julien Villeneuve (julien.villeneuve@igf.cnrs.fr)

Phone number: (+33) 4 34 35 93 36

Running title: A new assay for unconventional secretion

Keywords: secretory pathway, unconventional protein secretion, intracellular compartments, protein trafficking, intercellular communication, split luciferase, Tau, neurodegenerative diseases.

Synopsis: In this study, Denus et al. develop a powerful and highly customizable split luciferase-based assay allowing the analysis of multiple cargo proteins released by unconventional protein secretion. This assay provides a robust platform to address fundamental questions in the field of protein trafficking and secretion and advance our understanding of cellular communication.

Abstract

In addition to the conventional endoplasmic reticulum (ER)-Golgi secretory pathway, alternative routes are increasingly recognized for their critical roles in exporting a growing number of secreted factors. These alternative processes, collectively referred to as unconventional protein secretion (UcPS), challenge traditional views of protein and membrane trafficking. Unlike the well-characterized molecular machinery of the conventional secretory pathway, the mechanisms underlying UcPS remain poorly understood. Various UcPS pathways may involve direct transport of cytosolic proteins across the plasma membrane or the incorporation of cargo proteins into intracellular compartments redirected for secretion. Identifying the specific chaperones, transporters, and fusion machinery involved in UcPS cargo recognition, selection and transport is crucial to decipher how cargo proteins are selectively or synergistically directed through multiple secretory routes. These processes can vary depending on cell type and in response to particular stress conditions or cellular demands, underscoring the need for standardized tools and methods to study UcPS. Here, we combine the sensitivity of split NanoLuc Binary Technology with the versatility of the Retention Using Selective Hooks (RUSH) system, to develop a straightforward and reliable cell-based assay for investigating both conventional and unconventional protein secretion. This system allows for the identification of intracellular compartments involved in UcPS cargo trafficking. Additionally, its sensitivity enabled us to demonstrate that disease-associated mutants or variants of Tau and superoxide dismutase-1 (SOD1) show altered secretion via UcPS. Finally, we leveraged this assay to screen for Alzheimer's disease risk factors, revealing a functional link between amyloid-beta production and Tau UcPS. This robust assay provides a powerful tool for increasing our knowledge of protein secretion mechanisms in physiological and pathological contexts.

Introduction

In eukaryotic cells, the mechanisms by which secreted factors reach the extracellular space to exert their biological functions are more diverse than originally thought. Indeed, the traditional view that all secreted proteins contain an N-terminal signal sequence that directs them through the endoplasmic reticulum (ER)-Golgi secretory pathway, has been challenged by seminal discoveries (1–3). These findings highlight the existence of "unconventional protein secretion" (UcPS), a set of processes that export outside the cells numerous cytosolic proteins lacking a signal sequence for ER entry (4–10). These includes various inflammatory cytokines, annexins, heat shock proteins, lipid chaperones, galectins, and aggregate-prone proteins, among others.

While it is tempting to hypothesize that UcPS is governed by common principles akin to the evolutionarily conserved ER-Golgi pathway (11), recent research indicates a higher level of diversity and heterogeneity within UcPS mechanisms and the existence of several UcPS routes. In type I and II UcPS, proteins are directly translocated across the plasma membrane (PM) via protein channels and ABC transporters, respectively (12,13). In contrast, type III UcPS involves the incorporation of cytosolic proteins into intracellular compartments such as autophagosomes, endosomes, multivesicular bodies (MVBs) or lysosomes, which are then redirected for secretion by acquiring exocytosis properties (14–19). In some cases, type III UcPS also triggers the formation of vesicular intermediates *de novo* in response to cellular stresses. A notable example is the biogenesis of the compartment for unconventional protein secretion (CUPS) in yeast under starvation conditions, which is crucial for the export of proteins such as acb1, SOD1 and thioredoxins (20–23). Additionally, in type IV UcPS, ER-localized transmembrane proteins can bypass the Golgi apparatus and directly reach the PM (24,25). Cytosolic proteins can also be transported to neighboring cells through microvesicles or tunnelling nanotubes (TNTs) generated at the PM (26–29). Despite the diversity of UcPS mechanisms, common players and hubs are also emerging, suggesting the potential for a more unified understanding of these processes. Key players, such as the GRASP protein family and its orthologs, have been identified as crucial factors in the export of various cargo proteins through both type III and IV UcPS across multiple organisms, from yeast to mammals (3,20,30–33). Lysosomes have also emerged as multifunctional organelles at

the intersection of several intracellular trafficking pathways, serving as a convergence point for many cargo proteins in type III UcPS and in TNT-mediated intercellular communication (9,15,19,27,34–38).

Despite the central role of UcPS in physiological and pathological conditions (35,36,39,40), most of the underlying mechanisms remain poorly understood. Key challenges include unraveling the conserved and context-specific molecular mechanisms, identifying the regulatory factors that govern UcPS processes, and characterizing the amino acid motifs that direct cargo recognition and selection. Additionally, understanding how intracellular compartments are repurposed for secretion and exploring the evolutionary origins and adaptations of UcPS are crucial for advancing our knowledge in this field.

One major obstacle in studying UcPS is the relatively low amounts of secreted proteins compared to the total intracellular pool of the same protein. To circumvent this limitation, studies often extend secretion period to 1-2 days. This can result in cell detachment, stress, and cytosolic leakage, which can interfere with the detection of active UcPS processes. Current detection methods also face limitations. Techniques like Western blotting may lack sensitivity, while Enzyme-linked immunosorbent assays (ELISA) and Homogeneous time resolved fluorescence (HTRF) assays can be expensive and require the use of specific high-affinity antibodies. Immunoprecipitation is time-consuming, and quantitative mass spectrometry is not scalable for high-throughput analysis. Here, we developed an assay based on a luminescent reporter that offers high sensitivity, low cost, simplicity, versatility, and scalability for high-throughput applications. Additionally, we integrated a trapping approach to identify the compartments through which UcPS cargos transit for their export, particularly in type III UcPS. By analyzing diverse cargos, including those trafficked via specific UcPS pathways and those linked to neurodegenerative diseases, we demonstrate the relevance and broad applicability of this assay. This new cell-based assay represents a powerful tool to address key challenges in the study of UcPS and offers new opportunities for understanding its role in both physiological and pathological contexts.

Results

A quantitative luminescent assay to monitor conventional and unconventional protein secretion.

Using human SH-SY5Y neuroblastoma cells, we generated several lines stably expressing a specific cargo protein fused with the HiBit sequence. These cargo proteins included tumor necrosis factor-α (TNFα), a proinflammatory cytokine containing an N-terminal signal sequence that is secreted via the conventional ER-Golgi pathway (41), as well as several proteins that lack a signal sequence for ER entry, which have been reported to be secreted via UcPS. These include fibroblast growth factor-2 (FGF2), the best-characterized example of type I UcPS cargo protein (42), interleukin-1β (IL1β) and galectin-3 (Gal3), which both are known to be secreted through type I and III UcPS (14,43–45). Additionally, we included three proteins associated with neurodegenerative diseases and secreted via type III UcPS, namely α-synuclein (αSNC), superoxide dismutase-1 (SOD1) and Tau (36,46,47). Recent studies suggested that Tau may also be secreted by type I UcPS (48,49). A cell line expressing green fluorescent protein (GFP) fused to the HiBit sequence was also generated and used as a negative control. The HiBit tag, an 11-amino-acid peptide, has high affinity for its larger subunit, LgBit. Upon interaction, this reconstituted complex exhibits luciferase activity enabling split luciferase complementation assays (50) (**Fig. 1A & B**). Each cargo protein was also fused with streptavidin-binding protein (SBP), allowing the use and the adaptation of the retention using selective hook (RUSH) system through streptavidin (Strep)-SBP interaction (51). Western blotting of total cell lysates with an anti-HiBit antibody confirmed the correct expression of each cargo protein with the expected molecular weight migration shift, accounting for their fusion with the HiBit and SBP tags (**Fig. 1C**). To monitor protein secretion, cells were incubated in complete medium for 12 hours, followed by luciferase activity quantification in both cell lysates and media. The assay demonstrated high sensitivity, with a signal-to-noise ratio exceeding two-logs for all cargo proteins (**Fig. 1D & E**). Kinetic experiments also revealed a time-dependent increase in luminescence in the culture media for all cargo proteins, except for GFP, which did not increase over time, demonstrating the assay's specificity (**Fig. 1F, upper panel**). Importantly, the increase in extracellular luminescence was not due to cytosol leakage, as extracellular lactate dehydrogenase (LDH) activity remained unchanged (**Fig. 1F, bottom panel**). The comparison of

multiple UcPS cargos *vs.* GFP, combined with kinetic data and the lack of LDH release, confirmed that the developed assay can distinguish between active and specific UcPS-mediated secretion and non-specific protein release due to cell lysis or stress.

To further validate the assay, we examined the effect of brefeldin A (BFA), a chemical inhibitor of protein transport through the ER-Golgi membranes. BFA induces the fusion of Golgi membranes with the ER and endosomes, and the relocation of peripheral Golgi matrix proteins such as GM130 and GORASP2 to the ER exit site (52–54) (**Fig. 2A**). As expected, BFA treatment reduced TNFα secretion, consistent with its transport via the conventional ER-Golgi pathway. In contrast, the secretion of UcPS cargos, which occurs independently of the ER-Golgi route, remained unaffected (**Fig. 2B**). Similar results were observed in cells depleted of SCFD1, a key regulator of soluble N-ethylmaleimide-sensitive-factor attachment protein receptor (SNARE) complex assembly and ER-Golgi trafficking (55) (**Fig. 2C & D**).

Given that UcPS cargo proteins can be released into the extracellular space either in free form or enclosed within extracellular vesicles (45–47,56), we sought to determine whether our split luciferase complementation assay could distinguish between these different secreted forms. The cell-conditioned medium was collected after 12 hours and incubated with or without digitonin, a detergent used to permeabilize membranes. In the absence of digitonin, only the free form of the protein is quantified. In the presence of digitonin, vesicle-enclosed reporters become accessible to LgBit, allowing the measurement of the total amount of secreted protein. The addition of digitonin did not significantly increase luciferase activity for TNFα, which is secreted via the fusion of post-Golgi transport carriers with the PM (51), indicating that TNFα is not encapsulated within extracellular vesicles (**Fig. 2E**). Similar results were obtained for FGF2 and IL1β, suggesting that these UcPS cargo proteins, like TNFα, are released into the extracellular space in their free forms (**Fig. 2E**). Consistent with previous reports (45–47,56), a significant fraction of Tau, αSNC, SOD1, and Gal3 (11 %, 14 %, 22 % and 23 %, respectively) was secreted within vesicular structures, in addition to the main pool released in free form, as evidenced by the increase in luciferase activity upon addition of digitonin to the medium (**Fig. 2E**).

Altogether, these results demonstrate that the engineered cell lines expressing distinct HiBit- and SBP-fused cargo proteins enabled us to establish a quantitative, versatile, and sensitive cell-based assay to monitor protein secretion through both conventional and unconventional pathways, providing a straightforward and reliable method to study these processes.

A trapping strategy using the RUSH system to identify intermediate compartments in UcPS.

We next explored whether the split luciferase assay, in combination with the RUSH system, could be used to identify the intracellular compartments involved in UcPS. The RUSH system relies on a "hook", consisting of a resident protein of a specific organelle fused to Strep, and a "reporter", the cargo protein of interest fused with SBP (51). Upon co-expression, the reporter binds to the hook via the Strep-SBP interaction (**Fig. 3A)**. This interaction can be disrupted by the addition of biotin, which competes for Strep with high affinity (51). To implement this method, SH-SY5Y cells stably expressing Tau, IL1β, FGF2, or TNFα (each fused to the HiBit sequence and SBP) were transduced with a lentivirus to express a hook consisting of Strep fused N-terminally to a signal sequence and C-terminally to the KDEL motif, leading to Strep-KDEL hook localization within the ER lumen (**Fig. 3A).** As expected, without biotin, this setup trapped TNFα, a signal sequence-containing cargo protein, preventing its secretion. Upon the addition of biotin, which disrupts the Strep-SBP interaction, TNFα secretion was restored (**Fig. 3B)**. Conversely, when cells were transduced to express Strep fused with the invariant chain (Ii) at the N-terminal, resulting in a hook localized at the ER but with Strep oriented towards the cytosol (51), TNFα secretion was unaffected, with or without biotin (**Fig. 3B).**

We next applied these trapping strategies to SH-SY5Y cells expressing UcPS cargo proteins (FGF2 and Tau) that lack a signal sequence for ER entry. Expression of the Strep-KDEL hook with Strep oriented within the ER lumen did not impact the secretion of either FGF2 or Tau, regardless of the presence or absence of biotin (**Fig. 3C & D**). However, when the hook was localized in the ER with Strep facing the cytosol (Ii-Strep), secretion of both FGF2 and Tau was inhibited. This inhibition was reversed by biotin, confirming that their UcPS does not involve transport through the ER-ERGIC-Golgi axis (**Fig. 3C & D**).

We extended this analysis to IL1β, another UcPS cargo protein that lacks a signal sequence for ER entry. Similar to FGF2 and Tau, IL1β secretion was blocked by the cytosol-oriented Ii-Strep hook, with secretion restored upon biotin addition (**Fig. 3E**). However, the Strep-KDEL hook, which blocked TNFα secretion, also partially inhibited IL1β secretion (**Fig. 3E**). These results suggest that a fraction of IL1β may transit through compartments associated with the conventional secretory pathway. This is consistent with recent studies indicating that IL1β secretion is mediated by the TMED10-channeled UcPS (THU) pathway, which relies on TMED10 oligomerization to form a channel that facilitates UcPS cargo translocation into the ER-Golgi intermediate compartment (ERGIC) (57–59). Although the Strep-KDEL hook mainly localizes within the ER lumen (51), a small fraction may escape to the ERGIC and Golgi membrane before being retrieved back to the ER (60,61). This could explain its inhibitory effect on IL1β secretion, assuming IL1β is exclusively translocated into the ERGIC during THU-mediated UcPS (57–59).

Overall, our findings demonstrate that combining the NanoLuc Binary Technology with the RUSH system allows for the identification of intermediate compartments involved in UcPS, as evidenced by our results for IL1β which was previously identified to traffic through the ERGIC for its release (57). This highlights the potential of this method to reveal key steps and vesicular intermediates in UcPS pathways.

Impact of SOD1 and Tau mutations linked to familial amyotrophic lateral sclerosis and tauopathies on their UcPS.

SOD1 and Tau proteins have garnered significant attention as pathological aggregate-prone proteins which accumulate in neurodegenerative disease like amyotrophic lateral sclerosis (ALS) and tauopathies, such as Alzheimer's disease and frontotemporal dementia. Evidence shows that SOD1 and Tau can spread from cell to cell after their release via UcPS (47,56). Under proteotoxic stress, often associated with lysosomal degradative dysfunction (9,27), UcPS of these proteins may serve as an alternative pathway for clearing toxic materials, thereby preventing excessive cellular stress (36,37,56). However, this process may also have the potential to cause propagation of toxic materials between cells,

favoring disease progression at the organism level (27,48). We investigated whether disease-associated SOD1 and Tau mutations affect the UcPS-mediated intercellular spreading of these proteins using our cell-based assay. We first generated five SH-SY5Y cell lines expressing wild-type (wt) SOD1 and four SOD1 variants associated with familial ALS: G93A, D90A, A4V, and D76Y, each fused to the HiBit sequence and Strep (**Fig. 4A**). These mutations vary in their impact on SOD1 folding, function, aggregation and disease severity. The G93A, D90A and A4V mutations disrupt SOD1 folding and impair structural stability (62). Notably, the A4V mutation, one of the most aggressive mutations, severely reduces SOD1 stability and enzymatic activity, leading to increased aggregation propensity and rapid disease progression. The G93A mutation induces a toxic gain of function, causing SOD1 misfolding and aggregation, and is associated with severe neurodegeneration. In contrast, the D90A variant retains most of SOD1 enzymatic activity, though this varies among patients, leading to a milder clinical course. The D76Y mutation reduces the net repulsive charge of SOD1, affecting SOD1 electrostatic repulsion toward other molecular components. This mutation can also affect SOD1 stability and is associated to a very slow disease progression (62). Whether SOD1 mutations affect its secretion through UcPS remains to be elucidated. Western blot analysis of total cell lysates confirmed the expression of all SOD1 variants, although mutant forms exhibited lower expression levels compared to the wt, the most important reductions being observed for SOD1-G93A and SOD1-A4V (**Fig.4B**). To evaluate the secretion of these variants, cells were cultured in complete medium for 12 hours, and their release was measured using our split luciferase complementation assays. No difference was detected between the secretion of wt-SOD1 and D90A SOD1. However, the D76Y mutation decreased SOD1 secretion, whereas the G93A and A4V mutations promoted SOD1 secretion (**Fig. 4C, top panel**). Importantly, while LDH assays revealed no changes in cytosolic leakage for most of the SOD1 variants, confirming that the observed differences are due to altered secretion and not cell lysis, the G93A mutation clearly increased cellular stress, as evidenced by the higher activity of LDH detected in the medium of the corresponding cells (**Fig. 4C, bottom panel**). These findings indicate that SOD1 mutations not only influence protein stability, activity, and aggregation but also significantly affect its secretion via UcPS.

We next generated SH-SY5Y cell lines expressing several Tau variants, each fused to the Strep tag and HiBit sequence. These variants included S422E, Δ421, D421A, P301S, and a Tau variant in

which 14 serine/threonine residues were substituted with glutamate (E14), to mimic phosphorylation on these residues (48,63) (**Fig. 4D**). Indeed, Tau undergoes various post-translational modifications, including extensive phosphorylation on multiple residues, which critically modulates its function and interaction with microtubules (64,65). Notably, aggregated hyperphosphorylated Tau is the main component of the neurofibrillary tangles observed in the brain of Alzheimer's disease patients (66), and several studies suggest that phosphorylation promotes Tau secretion (48,67), with specific phosphorylated forms preferentially detected in the cerebrospinal fluid of Alzheimer's disease patients (68). The P301S mutation, associated with familial frontotemporal dementia (69), accelerates Tau aggregation (70). Similarly, the Δ421 mutation, which results in C-terminus truncation, is found in neurofibrillary tangles (71) and enhances Tau aggregation property (72). The D421A mutation prevents caspase-mediated cleavage at this site, preserving Tau full-length form, while the S422E mutation mimics phosphorylation at serine 422, a modification linked to inhibition of Tau cleavage at D421 and commonly found in aggregated Tau (73). Western blot analysis of total cell lysates showed relatively homogeneous expression levels of all Tau variants (**Fig. 4E**). As with the ALS-linked mutant SOD1, we cultured Tau-expressing cell lines in complete medium for 12 hours and assessed Tau secretion using the split luciferase complementation assay. The D421A and S422E mutations had no significant effect on Tau secretion, whereas the Δ421 and E14 variants promoted Tau UcPS (**Fig. 4F, top panel**). Importantly, no differences in LDH release were observed across the different cell lines, ruling out cell lysis as a confounding factor in Tau secretion variability (**Fig. 4F, bottom panel**). However, the increased secretion of P301S Tau was accompanied with an increase in LDH activity in the culture medium, suggesting that this variant undergoes non-specific release through cytosolic leakage (**Fig. 4F**).

Taken together, these results demonstrate that our assay allows the comparative analysis of different mutant forms of a given cargo protein. They also suggest that mutations in SOD1 and Tau can significantly affect their secretion via UcPS, potentially contributing to the pathogenesis of ALS and tauopathies.

Targeted screening of Alzheimer's disease risk genes reveals key factors in Tau UcPS.

The intercellular propagation of Tau in Alzheimer's disease highlights the crucial need to identify molecular factors that regulate Tau UcPS and their role in neurodegenerative disease progression. A promising avenue for increasing our understanding of Alzheimer's disease is to investigate whether risk genes associated with the disease influence Tau UcPS. To explore this issue and further validate the robustness of our cell-based split luciferase complementation assay, we conducted a targeted screen of Alzheimer's disease risk genes to assess their role in Tau secretion through UcPS. We designed 96-well plates pre-arrayed with a selection of specific smart pool siRNAs targeting 46 distinct Alzheimer's risk genes (74). These genes represent key players in cellular processes associated with neurodegeneration, including amyloid precursor protein (APP) processing, membrane trafficking, and protein degradation (74–84). Gene knockdowns were performed in SH-SY5Y cells expressing wt-Tau fused to the HiBit sequence and Strep tag. Three days after siRNA transfection, cells were washed and incubated for 12 hours in complete medium, and both cell lysates and medium were then harvested for split luciferase complementation assay (**Fig. 5A**). Our screen revealed that the knockdown of several genes modulated Tau UcPS. These included, for example, angiotensin I converting enzyme (ACE), ADAM metallopeptidase domain 10 (ADAM10), charged multivesicular body protein 2B (CHMP2B), Cas scaffold protein family member 4 (CASS4), WW domain-containing oxidoreductase (WWOX) and Gelsolin (GSN). (**Fig. 5B & Fig. S1A**). Interestingly, the knockdown of APP, as well as several genes that act along the endolysosomal pathway and involved in APP processing and amyloid-beta (Aß) production, strongly impacted Tau UcPS. These included ATP-binding cassette subfamily A member 7 (ABCA7) (75), bridging integrator 1 (BIN1) (76), presenilin 2 (PSEN2) (83) and valosin-containing protein (VCP) (84), among others (**Fig. 5B & Fig. S1A**). Importantly, when the same screen was performed in SH-SY5Y cells expressing Gal3 fused to the HiBit sequence and Strep tag, no significant changes in Gal3 UcPS were observed upon knockdown of these genes (**Fig. 5B & Fig. S1B**). These findings suggest that the amyloidogenic processing of APP, a critical event in Alzheimer's pathology leading to Aß generation (85), and/or the associated endolysosomal stress (86,87) may play a direct role in regulating Tau UcPS and, more broadly, contribute to Tau propagation and disease progression in Alzheimer's disease.

Amyloid-beta (Aß) peptide promotes Tau UcPS

APP is a transmembrane protein containing a signal sequence, which allows its transport to the PM via the conventional ER/Golgi secretory pathway. At the cell surface, APP undergoes proteolytic cleaved by the α-secretase, generating a neurotrophic factor through the so-called non-amyloidogenic pathway (88). Under pathological conditions such as Alzheimer's disease, APP can be internalized through endocytosis and trafficked via the endolysosomal pathway. Within this pathway, sequential cleavages by the β- and γ-secretases lead to the generation of Aß peptides. The secretion and aggregation of Aß peptides contribute to the formation of extracellular plaques, a hallmark of Alzheimer's disease (85,88). Given that several Alzheimer's disease risk factors, including BIN1, ABCA7, PSEN2 and VCP, are known to modulate Aß peptide production and also influence Tau UcPS (as shown in **Fig. 5B)**, we hypothesized that the amyloidogenic pathway and Aß generation within the endolysosomal pathway may promote Tau UcPS. To test this hypothesis, we incubated SH-SY5Y cells expressing wt-Tau fused to the Strep tag and HiBit sequence with 1 μM recombinant, fluorescently labeled Aß peptide. After 24 hours incubation, we confirmed that the recombinant Aß peptide was internalized and localized within the endolysosomal pathway, as shown by its colocalization with LAMP1 (**Fig. 5C**). Under these conditions, the split luciferase complementation assay revealed that the presence of recombinant Aß peptide significantly enhanced Tau UcPS compared to control cells incubated with a scramble peptide (**Fig. 5D**). Notably, Aß peptide had no effect on Gal3 UcPS (**Fig. 5E**). Furthermore, LDH assays showed no changes in cytosolic leakage, confirming the absence of non-specific cell damage in these experiments (**Fig. 5D & 5E, bottom panels**). Altogether, these results strongly suggest that Aß peptide may play a direct role in regulating Tau UcPS, establishing a functional link between two critical processes in Alzheimer's disease progression: Aß production and Tau dissemination.

Discussion

The diversity of UcPS pathways – whether involving direct translocation of cargo protein across the PM or their initial incorporation into intracellular compartments – along with the wide array of secreted factors produced by various cell types in response to stress or cellular demand (4,7,12,89), underscores the need for standardized assays with well-controlled experimental settings to decipher mechanisms underlying UcPS. Here, we developed a quantitative and versatile cell-based assay that accurately measures the secretion of multiple UcPS cargo proteins. A key issue in studies on UcPS is ensuring that signal detection from proteins released in the extracellular medium is not the result of cell death or PM permeabilization. While traditional controls such as LDH assays or the detection of intracellular markers like actin, tubulin, or GAPDH are useful, the ability to perform comparative and parallel analyses of different cargo proteins enhance the reliability and robustness of the data. By minimizing potential confounding effects from cell lysis or death across various experimental conditions, this approach can provide strong evidence for the specificity of distinct secretory pathways.

Overall, our split luciferase-based assay is highly customizable, allowing the analysis of multiple cargo proteins across various cell lines. Its sensitivity and adaptability to different assay formats make it an excellent tool for targeted genetic and pharmacological screening. Furthermore, the assay can distinguish between free proteins and those encapsulated in extracellular vesicles, enhancing its versatility for studying UcPS. A key added value in our assay is the integration of the RUSH system. Originally designed to study protein trafficking through the ER-Golgi pathway (51), the RUSH system is also highly relevant for analyzing proteins lacking a signal sequence and for identifying intermediate compartments involved in UcPS. Consistent with previous findings (57), our RUSH-integrated assay provides evidence that a fraction of IL1β is released following its trafficking through compartments of the conventional secretory pathway. This aligns with the THU pathway, a seminal discovery in the field (57,59,90). However, our results indicate that the THU pathway is not required for the secretion of other UcPS cargo proteins examined, such as Tau and FGF2. For proteins secreted via type III UcPS, the assay can be customized by targeting hook proteins to specific intracellular compartments. This flexibility allows the mapping of intermediate compartments through which cargo proteins traffic before secretion, providing valuable insights into the diverse pathways of UcPS.

An emerging area of research focuses on the role of UcPS in the progression of neurodegenerative diseases. The intracellular accumulation of toxic, misfolded proteins like SOD1 and Tau is a hallmark of several neurodegenerative diseases. These misfolded proteins not only accumulate within cells in a cell-autonomous manner but also spread intercellularly along neuroanatomical tracts (91,92). Evidence indicates that the release and transmission of aggregate-prone proteins, such as SOD1 in ALS and Tau in Alzheimer's disease and frontotemporal dementia, occurs via UcPS pathways (47,48). While most cases of these diseases are sporadic and arise from a combination of genetic, environmental and lifestyle factors, familial forms also exist, often driven by mutations in SOD1 and Tau (62,74). Our results indicate that mutations in SOD1 and Tau gene not only affect protein folding and activity, but also may contribute to ALS and tauopathy pathogenesis by altering their UcPS. For instance, the A4V SOD1 mutation, associated with rapidly progressive ALS (62), enhances SOD1 UcPS, whereas the D76Y mutation, linked to slower disease progression (62), reduces it. Interestingly, the D76Y mutation, which alters the net charge of SOD1 and its electrostatic interaction with other proteins, affects a diacidic motif previously identified as essential for SOD1 UcPS (22,93). While this motif could be viewed as indirectly influencing UcPS, it is highly conserved across SOD1 orthologs from yeast to mammals and also in the yeast acb1 protein, where it similarly regulates acb1 secretion via UcPS (22). This conservation suggests that the D76 residue is part of a broader motif critical for exporting several UcPS cargo proteins. Given its role in modulating SOD1 net repulsive charge, it is likely that under conditions of proteotoxic stress and protein conformational changes, exposure of this motif facilitates cargo recognition and selection by recruiting specific binding partners. Our results also underscore the significance of post-translational modifications, such as phosphorylation, in regulating Tau UcPS (48,67). Together, these results suggest a subtle and complex interplay between the physicochemical properties of protein variants and their export via UcPS, with potential implications for disease progression and severity. A deeper understanding of these structure-UcPS-disease relationships is essential. Future research should also explore whether different forms of the same UcPS cargo protein utilize distinct or overlapping secretory pathways and how these pathways may act synergistically during cellular stress. For instance, IL1β secretion occurs via both type I and type III UcPS pathways,

409 depending on the intensity and duration of inflammatory stress (44,94). In this context, our quantitative
410 UcPS assay could serve as a powerful tool to identify *cis* motifs essential for cargo selection and
411 recognition, as well as *trans* effectors such as chaperones that direct cargo to specific secretory routes.
412
413 Finally, our assay for screening Alzheimer's disease risk factors has proven to be a powerful
414 tool in identifying modifiers of Tau secretion and in establishing a functional link between Aß peptide
415 generation and Tau UcPS. The progression of Alzheimer's disease involves two key sequential
416 pathogenic processes. The first is the deposition of Aß peptide, which can occur during the early stages
417 of the disease without necessarily being associated with neurodegeneration. The second involves Tau
418 aggregation and spreading, typically linked to neuronal dysfunction and loss (95). A major challenge in
419 connecting these processes is their distinct subcellular localization and topological organization. APP is
420 a transmembrane protein trafficked to the PM via the ER-Golgi secretory pathway, where it can be
421 internalized and proteolytically cleaved within endolysosomal compartments to generate Aß peptide
422 (85,88). In contrast, Tau is a cytosolic protein that primarily associates with microtubules but can be
423 secreted via UcPS (48). Interestingly, recent studies suggest that Tau and other aggregate prone-proteins
424 can also be incorporated into endolysosomal compartments, which may be redirected for secretion under
425 proteotoxic stress (36,96–100). Our data indicate that Aß peptides regulates Tau UcPS. This leads us to
426 hypothesize that Aß peptide generation within endolysosomal compartments, along with the associated
427 proteotoxic stress, alters their dynamics and function. Consequently, these compartments may be
428 rerouted to the PM for exocytosis, releasing their contents, including Tau, into the extracellular space.
429 It is likely that only a subset of these compartments is redirected for secretion, probably those in which
430 the combined effects of Aß and Tau surpass a critical proteotoxic stress threshold. This would overwhelm
431 the endolysosomal system capacity to maintain its integrity and homeostasis (9), triggering Tau
432 pathology and facilitating its spreading through endolysosomal-mediated UcPS (**Fig. 5F**). In summary,
433 the interplay between Aß peptide generation and Tau incorporation into the endolysosomal pathway may
434 establish and perpetuate a pathological cycle, potentially explaining the sequential progression of
435 Alzheimer's disease. This model provides a valuable framework for further exploring the role of
436 endo/lysosomes and UcPS in Alzheimer's disease pathogenesis (9,86,101).

In conclusion, the field of UcPS is rapidly evolving, with ongoing research aimed at uncovering its intricate mechanisms, its role in health and disease, and its therapeutic potential. While the development of *in vivo* models that accurately recapitulate the molecular and cellular dynamics of UcPS remains a significant challenge, our versatile assay provides a robust platform to address fundamental questions in the field and advance our understanding of cellular communication.

Materials and Methods

Antibodies, reagents and plasmids

Antibodies used in this study included: mouse monoclonal antibodies anti-HiBit (Promega, #CS2006A01), anti-GM130 (BD Biosciences, #610823), anti-GAPDH coupled to HRP (Cell Signaling, #51332s), anti-Actin coupled to HRP (Invitrogen, #MA5-11869), rabbit monoclonal antibody anti-LAMP1 (Cell Signaling, #9091s), anti GORASP2 (ProteinTech, #10598-1-AP), secondary antibodies donkey anti-sheep IgG-Alexa Fluor 594 (Invitrogen, #A11016), goat anti-mouse IgG-Alexa Fluor 488 (Invitrogen, #A11029), goat anti-mouse IgG-546 (Invitrogen, #A11030), secondary antibody mouse IgGκ conjugated to HRP (Jackson Immuno Research, #115-035-174).

Reagents used in this study were obtained from the following sources. Dulbecco's modified Eagle's medium ((DMEM), Sigma, #D8437), Dulbecco's phosphate buffered saline (D-PBS, Sigma, #D8537), MEM Non-essential amino acid solution (Sigma, #M7145), Penicillin/Streptomycin (Gibco, #15140-122), L-glutamine (Sigma, #G7513), Fetal bovine serum ((FBS) Gibco, #10270-106), Trypsin (Gibco, #25300-054), Puromycin (Sigma, #P9620), G-418 (Sigma, #4727878001), OptiMEM (Gibco, #31985-062), BFA (Sigma, #B6542), Universal mycoplasma detection kit (ATCC, #ATCC®30-1012K™), View plate™ 96F TC (Black, Clear bottom, PerkinElmer #6005182), Lipofectamine®2000 transfection reagent (Invitrogen, #11668019), *Trans*IT®-2020 transfection reagent (Mirus, #MIR5400), Polybrene (Millipore Corp, #TR-1003-G), 0.45µm low protein binding membrane (VWR International, #28145-479), Protease inhibitor cocktail (Sigma, #11836170001), Dako fluorescent mounting medium (Agilent, # S3023), Dapi (4,6-diamidino-2-phenylindole; ThermoFisher, #P36935), Mini-protean TGX stain free gels 4-20% (Biorad, #4561094), TransBlot Turbo Midi-Size Nitrocellular membrane (BioRad, #1704271), ECL Western Blotting Detection Reagent (Biorad, #170-5061 and GeneTex, #GTX14698), Nano-Glo® HiBit Extracellular Detection system (Promega, #N2421), Nano-Glo® HiBit Lytic Detection system (Promega, #N3040), Lactate Dehydrogenase assay kit (Abcam, #ab102526), Color prestained protein standard (Biolabs, #P7719S), β-amyloïd (1-42) Hilyte TM Fluor 555-labeled (Anaspec, #AS-60480-01), β-amyloïd 1-42 (Anaspec, #AS-20276), scramble-β-amyloïd 1-42 (Anaspec, #AS-25382).

Plasmids included pcDNA3.1-GFP-2A-HiBit-Tau, pcDNA3.1-GFP-2A-HiBit-αSNC, pcDNA3.1-GFP-2A-HiBit-Gal3, pcDNA3.1-GFP-2A-HiBit-PAUF, pcDNA3.1-GFP-2A-HiBit-IL1β, pcDNA3.1-GFP-2A-HiBit-FGF2, pcDNA3.1-GFP-2A-HiBit-SOD1, pcDNA3.1-GFP-2A-HiBit-EGFP, pcDNA3.1-GFP-2A-HiBit-SOD1-A4V, pcDNA3.1-GFP-2A-HiBit-SOD1-D76Y, pcDNA3.1-GFP-2A-HiBit-SOD1-G90A, pcDNA3.1-GFP-2A-HiBit-SOD1-G93A, pcDNA3.1-GFP-2A-HiBit-Tau-E14, pcDNA3.1-GFP-2A-HiBit-TauD421A, pcDNA3.1-GFP-2A-HiBit-Tau-P301S, pcDNA3.1-GFP-2A-HiBit-Tau-D422E, pcDNA3.1-GFP-2A-HiBit-Tau-Δ421 (ThermoFisher scientific). pCDH-Str-KDEL-neomycin was a gift from Franck Perez (Addgene plasmid #65307; http://n2t.net/addgene:65307 ; RRID:Addgene_65307) (51). pCDH_Str-Ii was a gift from Franck Perez (Addgene plasmid # 65313; http://n2t.net/addgene:65313 ; RRID:Addgene_65313) (51).

Cell culture

The neuroblastoma cell line SH-SY5Y (ATCC) was grown in complete culture medium consisting of Dulbecco's modified Eagle's medium (DMEM, Sigma, #D8437) supplemented with 10% heat-inactivated FBS (Gibco, #10270-106), 100 U/ml penicillin, 100 µg/ml streptomycin (Gibco, #15140-122) and 2 mM L-glutamine (Sigma, #G7513) and maintained in humidified atmosphere containing 5% CO_2 at 37°C. The cells were tested every month using the Universal mycoplasma detection kit (ATCC, #ATCC®30-1012K™) to confirm the absence of mycoplasma contamination. To generate SH-SY5Y cell lines stably expressing the different cargo proteins fused to the HiBit and SBP, SH-SY5Y cells were transfected with the corresponding plasmids using *Trans*IT®-2020 transfection reagent (Mirus, #MIR5400), according to the manufacturer's recommendations. After two days, transfected cells were selected with 600 µg/ml G-418 (Sigma, #4727878001) for one week. GFP-positive cells were then isolated by fluorescence-activated cell sorting (FACS). After expansion into 6-well plate format, the cell lines were assessed by Western blotting analysis.

Split luciferase complementation assay

SH-SY5Y cells expressing the HiBit tagged reporter was cultured in a 96-well plates™ 96F TC (Black, Clear bottom, PerkinElmer #6005182) and incubated in complete medium for the indicated time. The split luciferase complementation assay was performed from 100 µL of cell culture medium using the Nano-Glo® HiBit Extracellular Detection System Kit (#N2421, Promega), and from 100 µL of cells permeabilized using the Nano-Glo® HiBit Lytic Detection System Kit (#N3040, Promega) according to manufacturer's instructions. This protocol is based on the established concept of bimolecular fluorescence complementation (BiFC), and detects reporter luciferase activity only after complementation in the presence of LgBiT. Luminescent signal was measured using a Tecan Microplate reader Infinite 500 at the Arpege pharmacological screening platform (Biocampus, UM-CNRS-INSERM, Montpellier, France). The ratio of medium to lysate luminescence was quantified and the values were normalized to the control sample for each condition.

siRNA-mediated knockdown

For specific single siRNA transfection with Smart pools siRNA, SH-SY5Y cells were transfected using Lipofectamine®2000 transfection reagent (Invitrogen, #11668019) according to the manufacturer's recommendations. Smart pools siRNAs were purchased from Dharmacon. The siRNA sequences used were ON-TARGETplus non-targeting pool (#D-001810-10-50) 5'-UGGUUUACAUGUCGACUAA-3', 5'-UGGUUUACAUGUUGUGUGA-3', 5'-UGGUUUACAUGUUUUCUGA-3', 5'-UGGUUUACAUGUUUUCCUA-3'. ON-TARGETplus human SCFD1 siRNA smart pool (#L-010943-01-0005) 5'-AAGCAUUGGUGCACGAUGU-3', 5'-GACAAGAAACUUCGAGAAA-3', 5'-GUGCCAGGAUCUUCGAAAU-3', 5'-GAUAUCACAGACACGGAAA-3'. Cells were reverse transfected with specific individual siRNAs (75 nM final concentration per well) in the culture medium without antibiotics. After 4-6 hours, the transfection medium was replaced with normal culture medium. After 24 hours, cells were forward transfected with 75 nM siRNA as before and cells were maintained in culture medium for two additional days. For the targeted screening of Alzheimer's disease risk genes, SH-SY5Y cells expressing either wt-Tau or Gal3 fused to the HiBit sequence and Strep tag were reverse transfected in 96-well plate pre-arrayed with specific smart pools siRNA (Dharmacon) targeting selected genes (**Supplemental Table**

1). Briefly, 5,000 SH-SY5Y cells suspended in 80 µl of complete medium without antibiotics were seeded into 96-well plates containing 20 µl of 250 nM siRNA and 0.5% (v/v) lipofectamine 2000 in OptiMEM (Gibco, #31985-062). After 4-6 hours, the transfection medium was replaced with normal culture medium. After 24 hours, cells were forward transfected and cells were maintained in culture medium for two additional days.

Cell death - cell lysis analysis

Lactate dehydrogenase (LDH) release was monitored from cell culture media collected at the indicated times to assess the extent of plasma membrane damage and cell death using a commercially available LDH assay kit (Abcam, #ab102526), according to the manufacturer's recommendations.

Lentivirus production and transduction

Lentivirus was produced by the vector core facility of Montpellier (Plateforme de Vectorologie de Montpellier, Biocampus, UM-CNRS-INSERM, Montpellier, France). Briefly, lentivirus was generated in HEK293T cells transfected using the calcium phosphate method. At 50% confluence, HEK293T cells grown in complete medium without penicillin/streptomycin were transiently transfected with a lentiviral vector, either pCDH-Str-KDEL (Addgene plasmid #65307) for Strep-KDEL protein expression with Strep directed to the ER lumen, or pCDH_Str-Ii (Addgene plasmid # 65313) for Strep-Ii protein expression with Strep directed to the cytosol, together with the HIV packaging plasmid psPAX2 and the plasmid pMD2G, which codes for the vesicular stomatitis virus envelope glycoprotein G. After transfection (24 h), the medium was refreshed, and after an additional 24 h, virus was collected and filtered through a 0.45µm low protein binding membrane (VWR International, #28145-479), and concentrated on sucrose by ultracentrifugation at 17,000xg for 1.5 h, at 4°C. 15 µL of virus was used to infect ~1 million target cells plated in a 10-cm dish to a final volume of 10 ml. Medium was supplemented with 8 µg/ml polybrene (Millipore Corp, #TR-1003-G) without penicillin/streptomycin. After 24 h, the medium was replaced with fresh medium, and after an additional 24 h incubation period, 2 µg/ml puromycin (Sigma, #P9620) was added to select transduced cells.

Western blotting

Cells were lysed for 30 min on ice in lysis buffer (50 mM Tris, pH 7.4, 150 mM NaCl, 0.1% SDS, 1% (v/v) Triton X-100 and 0.5% sodium deoxycholate) supplemented with a protease inhibitor cocktail (Sigma, #11836170001), 1 mM Na_3VO_4 and 25 mM sodium fluoride and centrifuged at 16,000xg for 15 min. Samples were incubated with 1X sodium dodecyl sulfate (SDS) sample buffer at 95°C for 10 min, resolved by SDS-PAGE using 4-20% Mini-protean TGX stain free gels 4-20% (Biorad, #4561094), and transferred to nitrocellulose membrane (BioRad, #1704271). Membranes were blocked with 5% (w/v) BSA in PBS containing 0.1% Tween 20 (PBS-T) for 30 min at room temperature, and incubated with appropriate primary antibodies overnight at 4°C in PBS-T containing 5% (w/v) BSA. The membranes were then washed 3 x 15 min in PBS-T and incubated with the appropriate HRP-conjugated secondary antibody for 1 h at room temperature in PBS-T containing 5% (w/v) BSA. The membranes were then washed again for 3 x 15 min in PBS-T and immunoreactive bands were detected with an enhanced chemiluminescence method (ECL Western Blotting Detection Reagent (Biorad, #170-5061 or GeneTex, #GTX14698)) and signal was acquired with a ChemiDoc MP Imaging System (Bio-Rad).

Immunofluorescence microscopy

Cells grown on coverslips were fixed with cold methanol for 10 min at -20°C or with 4% (w/v) PFA in PBS for 15 min at room temperature. Cells fixed with PFA were permeabilized with 0.1% Triton X100 in PBS at room temperature and then incubated with blocking buffer (2.5% (v/v) FCS, 0.1% Triton X100 in PBS) for 30 min at room temperature. Cells were then incubated with primary antibodies diluted in blocking buffer for 1 h at room temperature, followed by PBS wash and incubation with secondary antibodies. Secondary antibodies conjugated with Alexa Fluor 488 or 568 were diluted in blocking buffer and incubated for 1 h at room temperature. Samples were mounted using Dako fluorescent mounting medium (Agilent, # S3023) with Dapi (4,6-diamidino-2-phenylindole; ThermoFisher, #P36935). Images were acquired using a Leica SP8 laser confocal laser scanning microscope with a 40x objective at the imaging facility MRI (Biocampus, UM-CNRS-INSERM, Montpellier, France). Images displayed in the figures are representative single Z-slices. After

acquisition, images were processed using an Airyscan processing tool on the ZEN software provided by Zeiss.

Statistical analysis

The data represent the mean ± standard deviation (SD). Statistics were performed using the GraphPad Prism 10 software. Statistical tests were performed as specified in the figure legends. Results of the statistical analyses are displayed in the figures. P-Values < 0.05 were considered as statistically significant. *, $p<0.05$, **, $p<0.01$, ***, $p<0.001$, ****, $p<0.0001$.

Online supplemental material

Fig. S1 shows the detailed results of the split luciferase complementation assay performed in SH-SY5Y cells expressing Tau and Gal3, each fused to the HiBit sequence and Strep tag. These cells were transfected with siRNAs targeting Alzheimer's Disease risk genes. Table S1 provides the sequences of all smart pool siRNAs used for the targeted screening of Alzheimer's disease risk genes.

Figure legends

Figure 1: Sensitive and versatile cell-based assay for protein secretion. (A) Schematic representation of the plasmids used to generate the SH-SY5Y cell lines expressing different cargo proteins fused to the HiBit sequence and Strep tag. For all cell lines, the GFP tag, co-translationally self-cleaved with the 2A peptide, allowed selection of transduced cells by FACS (see "Materials and Methods"). Although not depicted in the schematic, the sequence encoding the signal sequence (ss) of TNFα has been inserted upstream of the sequence encoding SBP in the corresponding construct. **(B)** Schematic representation of the split luciferase assay. **(C)** Stable cell lines expressing cargo proteins, either TNFα, IL1β, FGF2, Gal3, Tau, αSNC, SOD1, and GFP fused to the HiBit sequence and Strep tag, were lysed and the corresponding extracts subjected to SDS-PAGE, followed by Western blotting with anti-HiBit and anti-β actin antibodies. Non-transduced SH-SY5Y cells were used as a negative control. Samples were loaded on each gel in duplicate. **(D & E)** Quantification of cargo protein secretion by split luciferase complementation assay from cell lysate (D) and medium (E) in non-transduced cells and cells expressing the different reporters. The sensitivity of the assay is confirmed by a signal-to-noise ratio above 2-log (mean of n = 3 ± SD; ***p≤0,001, ****p<0.0001 vs. non-transduced cells (Ctrl) analyzed by one-way ANOVA followed by Dunnett's multiple comparison test). **(F)** Split luciferase complementation assay in SH-SY5Y cells expressing the different cargo proteins incubated in complete medium in a 12-hour time course at 4-hour intervals. The ratio of medium to lysate luminescence was quantified and the values for each condition were normalized to t=4h. As a control, split luciferase complementation assay was performed in SH-SY5Y cells expressing GFP fused to the HiBit sequence and Strep tag (mean of n = 3 ± SD; ****p<0.0001 vs. EGFP luminescence when comparing slopes from linear regression model). LDH release was also monitored from each medium fraction (mean of n = 3 ± SD) and analyzed by two-way ANOVA followed by Dunnett's multiple comparison test. The specificity of the assay was validated by the luciferase activity, which increased over time for each cargo protein except for GFP, and by the absence of a difference in LDH release between all conditions.

Figure 2: UcPS cargo proteins are secreted independently of the ER-Golgi secretory pathway and are differentially released in extracellular vesicles. (A) Representative confocal images showing immunofluorescence staining of Golgi membrane (GM130 and GORASP55 in green) and nuclei stained with DAPI (blue) from SH-SY5Y cells incubated in DMSO or 500 ng/ml BFA for 12 hours. Scale bar: 10 µm. **(B)** Split luciferase complementation assay in stable SH-SY5Y cells expressing HiBit-tagged cargo protein incubated in complete medium in the presence of DMSO or 500 ng/ml BFA for 12 hours at 4-hour intervals. The ratio of medium to lysate luminescence was quantified and the values for each condition were normalized to the control sample (DMSO) at t=4h (mean of n = 3 ± SD; ****p<0.0001 vs. DMSO condition when comparing slopes from linear regression model). Bars in the bottom graphs indicate LDH release from each medium fraction (mean of n = 3 ± SD) analyzed by two-way ANOVA followed by Dunnett's multiple comparison test. **(C)** SH-SY5Y cells were transfected with ctrl siRNA or siRNA targeting SCFD1. 3 days after transfection, the knockdown efficiency of SCFD1 was assessed by Western blotting of total cell lysates with an anti-SCFD1 antibody. β actin was used as a loading control. Samples from 3 independent experiments were loaded on the same gel. **(D)** Split luciferase complementation assay in stable SH-SY5Y cells expressing HiBit-tagged cargo proteins transfected with ctrl siRNA and siRNA targeting SCFD1. Cells were incubated in complete medium for 12 hours at 4-hour intervals. The ratio of medium to lysate luminescence was quantified and the values for each condition were normalized to the control sample (ctrl siRNA) at t=4h (mean of n = 3 ± SD; ****p<0.0001 vs. DMSO condition when comparing slopes from linear regression model). Bars in the bottom graphs indicate LDH release from each medium fraction (mean of n = 3 ± SD) analyzed by two-way ANOVA followed by Dunnett's multiple comparison test. **(E)** Split luciferase complementation assay in medium collected after 12 hours from SH-SY5Y cells expressing HiBit-tagged cargo proteins. For each cell line, collected medium was incubated in the presence or absence of 30 µg/ml digitonin for 15 minutes on ice before luminescence quantification. For each experiment, values were normalized to medium samples incubated without digitonin (mean of n = 6 ± SD; *p≤0.05, **p≤0.01 vs. (–) digitonin, analyzed by Kolmogorov Smirnov's test).

Figure 3: The RUSH system revealed the role of conventional secretory pathway compartments in IL1β UcPS. (A) Left panel, schematic representation of the plasmids used for the RUSH system. Hooks include Strep-KDEL, with Strep facing the ER lumen, and Ii-Strep, also localized to the ER, but with Strep facing the cytosol. Reporters include TNFα, a cargo protein containing a signal sequence (ss), and three UcPS cargo proteins including IL1β, FGF2 and Tau, all fused to the HiBit sequence and SBP tag. Right panel, Schematic representation of the different configurations used for the RUSH system. In SH-SY5Y cells, expression of an ER hook with Strep facing the cytosol is expected to inhibit secretion of UcPS cargo protein and have no effect on secretion of cargo protein containing a signal sequence (ss) that is transported along the ER-Golgi secretory pathway. In contrast, the expression of an ER hook with Strep facing the ER lumen is expected to have no effect on the secretion of UcPS cargo protein, but to prevent the secretion of ss-containing cargo protein. Importantly, the inhibition of cargo protein secretion by the Strep-SBP interaction is prevented by the addition of biotin. **(B to E)** Split luciferase complementation assay in SH-SY5Y cells expressing an ER hook facing either the ER lumen or the cytosol, and cargo proteins fused to the HiBit sequence and Strep tag including TNFα (B), FGF2 (C), Tau (D), and IL1β (E). Cells were incubated for 12 hours in complete medium in the presence or absence of 30 μM biotin. The ratio of medium to lysate luminescence was quantified and the values for each condition were normalized to the control sample (cells expressing a luminal ER hook with biotin) (mean of n = 3 ± SD; **p≤0.01, ***p≤0.001, ****p<0,0001 vs. t=4h analyzed by two-way ANOVA followed by Tukey's multiple comparison test). Bars in the bottom graphs indicate LDH release from each medium fraction (mean of n = 3 ± SD) analyzed by two-way ANOVA followed by Tukey's multiple comparison test.

Figure 4: UcPS of SOD1 and Tau mutants/variants. (A) Left panel, schematic representation of the plasmids used to generate the SH-SY5Y cell lines expressing different SOD1 variants fused to the HiBit sequence and Strep tag. The SOD1 variants included SOD1-wt, SOD1-G93A, SOD1-D90A, SOD1-A4V, and SOD1-D76Y. Right panel, schematic representation of the split luciferase assay. **(B)** Stable cell lines expressing the different SOD1 variants fused to the HiBit sequence and Strep tag were lysed

and subjected to SDS-PAGE, followed by Western blotting with anti-HiBit, anti-SBP, anti-GFP, and anti-β actin antibodies. Non-transduced SH-SY5Y cells were used as a negative control. **(C)** Split luciferase complementation assay in SH-SY5Y cells expressing SOD1 variants fused to the HiBit sequence and Strep tag, incubated in complete medium for 12 hours. The ratio of medium to lysate luminescence was quantified and the values for each condition were normalized to the control sample (cells expressing SOD1-wt) (mean of n = 4 ± SD; **p≤0.01, ***p≤0.001, ****p<0,0001 vs. SOD1-wt analyzed by one-way ANOVA followed by Dunnett's multiple comparison). Bars in the bottom graphs indicate LDH release from each medium fraction (mean of n = 4 ± SD) ****p≤0.0001 analyzed by one-way ANOVA followed by Dunnett's multiple comparison test). **(D)** Left panel, schematic representation of the plasmids used to generate the SH-SY5Y cell lines expressing different Tau variants fused to the HiBit sequence and Strep tag. Tau variants included Tau-wt, Tau-S422E, Tau-Δ421, Tau-D421A, Tau-P301S, and Tau-E14. Right panel, schematic representation of the split luciferase assay. **(E)** Stable cell lines expressing the different Tau variants fused to the HiBit sequence and Strep tag were lysed and subjected to SDS-PAGE, followed by Western blotting with anti-HiBit, anti-SBP, anti-GFP, and anti-β actin antibodies. Non-transduced SH-SY5Y cells were used as a negative control. **(F)** Split luciferase complementation assay in SH-SY5Y cells expressing Tau variants fused to the HiBit sequence and Strep tag incubated in complete medium for 12 hours. The ratio of medium to lysate luminescence was quantified and the values for each condition were normalized to the control sample (cells expressing Tau-wt) (mean of n = 4 ± SD; ****p<0,0001 vs. Tau-wt analyzed by one-way ANOVA followed by Dunnett's multiple comparison test). Bars in the bottom graphs indicate LDH release from each medium fraction (mean of n = 4 ± SD) analyzed by one-way ANOVA followed by Dunnett's multiple comparison test.

Figure 5: Alzheimer's Disease risk factors and Aß peptide influence Tau UcPS. (A) Schematic representation of the targeted screening workflow. SH-SY5Y cell lines expressing either Tau or Gal3 fused to the HiBit sequence and Strep tag were reverse transfected in 96-well plates pre-arrayed with specific smart pool siRNA targeting Alzheimer's Disease risk genes. After 24 hours, cells were forward

transfected and cells were maintained in growth medium for another two days. Cells were then washed, incubated in complete medium, and after 12 hours, split luciferase complementation assay was performed on cell lysate and collected medium. **(B)** Heat map showing the results of the split luciferase complementation assay performed in SH-SY5Y cells expressing Tau and Gal3 fused to the HiBit sequence and Strep tag, transfected with siRNA targeting Alzheimer's Disease risk genes, and incubated in complete medium for 12 hours. The ratio of medium to lysate luminescence was quantified and the value in control sample (cells transfected with ctrl siRNA) was set as 1. Then, each value obtained with siRNA targeting Alzheimer's Disease risk genes was calculated relative to control sample (n = 4). The heat map shows the log2 value. Gene knockdowns that increase UcPS are noted in red, gene knockdowns that decrease UcPS are noted in blue. Detailed results are shown in Fig. S1. **(C)** Representative confocal images of SH-SY5Y cells incubated in the absence or presence of 1 µM fluorescent Aß peptide for 24 hours. Immunofluorescence staining of endo/lysosomes with anti-LAMP1 antibody (green) shows that Aß peptide (magenta) added to the culture medium is internalized and transported along the endocytic pathway. Nuclei are stained with DAPI (blue). Scale bar: 10 µm. **(D & E)** Split luciferase complementation assay in stable SH-SY5Y cells expressing Tau (D) and Gal3 (E) fused to the HiBit sequence and Strep tag and incubated in complete medium for 24 hours in the presence or absence of 1 µM Aß peptide or 1 µM scramble peptide. The ratio of medium to lysate luminescence was quantified and values for each condition were normalized to the control sample (cells incubated in the presence of scramble peptide) (mean of n = 5 ± SD; *p≤0.05 vs. scramble peptide (control condition) analyzed by Kolmogorov Smirnov's test). Bars in the bottom graphs indicate LDH release from each medium fraction (mean of n = 5 ± SD) analyzed by Kolmogorov Smirnov's test. **(F)** Schematic illustrating the potential functional link between the amyloidogenic pathway generating Aß peptide and Tau UcPS, a critical event for Tau propagation during Alzheimer's disease pathogenesis. Since it has been reported that toxic misfolded Tau can be incorporated into endo/lysosomal compartments, which can then fuse with the PM and contribute to Tau UcPS, we hypothesize that Aß peptide, along the endocytic pathway, may induce stressed endo/lysosomes and convert these organelles into secretory compartments.

Acknowledgments

J.V. acknowledges support from the Centre National de la Recherche Scientifique (CNRS), the Institut National pour la Santé et la Recherche Médicale (INSERM), the University of Montpellier (UM), the Association France Alzheimer et maladies apparentées, the Fédération pour la Recherche sur le Cerveau (FRC), the Fondation pour la Recherche Médicale (FRM – MND202310017892), and the Agence Nationale de la Recherche (ANR-23-CE16-0012) and (ANR-24-CE16-5161-02). M.L.P. acknowledges support from the Centre of Excellence in Neurodegeneration (CoEN) of Montpellier. S.E.S. acknowledges support from the Australian Research Council (DE200100611). DCR's work is supported by the UK Dementia Research Institute [through UK DRI Ltd, principally funded by the UK Medical Research Council, and The National Institute for Health Research Cambridge Biomedical Research Centre at Addenbrooke's Hospital. The views expressed are those of the author(s) and not necessarily those of the NHS, the NIHR or the Department of Health and Social Care. Split luciferase complementation assays were performed using the facilities of the Arpege pharmacological screening platform, viral productions were performed using the vector core facility of Montpellier (Plateforme de Vectorologie de Montpellier, PVM), and confocal microscopy analysis were performed using the imaging facility MRI, member of the national infrastructure France-BioImaging infrastructure supported by the French National Research Agency (ANR-10_INBS-04, "Investments for the future") (Biocampus, UM-CNRS-INSERM, Montpellier, France).

Author contributions

M.D., A.F., W.F., E.N.: Investigation, Validation, Formal analysis, Visualization; S.E.S.: Conceptualization, Methodology, Writing – Review & Editing; M.C., T.C.: Investigation; A.M., P.M., S.C., D.C.R.: Conceptualization, Methodology, Writing – Review & Editing; M.L.P, J.V.: Conceptualization, Methodology, Formal analysis, Writing – Original Draft, Writing – Review & Editing, Visualization, Supervision, Project administration, Funding acquisition. All authors approved the publication of this study.

Declaration of interest

D.C.R. is a consultant for Drishti Discoveries, PAQ Therapeutics, MindRank AI, Retro Biosciences, Alexion Pharma International Operations Limited, and Nido Biosciences. All other authors declare no competing interests.

References

1. Rubartelli A, Cozzolino F, Talio M, Sitia R. A novel secretory pathway for interleukin-1 beta, a protein lacking a signal sequence. EMBO J. 1990;9(5):1503–10.
2. Rubartelli A, Bajetto A, Allavena G, Wollman E, Sitia R. Secretion of thioredoxin by normal and neoplastic cells through a leaderless secretory pathway. J Biol Chem. 1992;267(34):24161–4.
3. Kinseth MA, Anjard C, Fuller D, Guizzunti G, Loomis WF, Malhotra V. The Golgi-associated protein GRASP is required for unconventional protein secretion during development. Cell. 2007 Aug;130(3):524–34.
4. Zhang M, Schekman R. Unconventional secretion, unconventional solutions. Science. 2013;
5. Rabouille C, Malhotra V, Nickel W. Diversity in unconventional protein secretion. J Cell Sci. 2012;
6. Dimou E, Nickel W. Unconventional mechanisms of eukaryotic protein secretion. Curr Biol. 2018;
7. Filaquier A, Marin P, Parmentier ML, Villeneuve J. Roads and hubs of unconventional protein secretion. Curr Opin Cell Biol. 2022 Apr 1;75:102072.
8. Chiritoiu-Butnaru M, Stewart SE, Zhang M, Malhotra V, Villeneuve J. Editorial: Unconventional protein secretion: From basic mechanisms to dysregulation in disease. Front Cell Dev Biol. 2022;10:1088002.
9. Néel E, Chiritoiu-Butnaru M, Fargues W, Denus M, Colladant M, Filaquier A, et al. The endolysosomal system in conventional and unconventional protein secretion. J Cell Biol. 2024 Sep 2;223(9):e202404152.
10. Denus M, Fargues W, Filaquier A, Néel É, Marin P, Parmentier ML, et al. [Unconventional protein secretion - new perspectives in protein trafficking]. Med Sci MS. 2024 Mar;40(3):267–74.
11. Schekman RW. Retrospective: George E. Palade (1912-2008). Science. 2008;
12. Rabouille C. Pathways of Unconventional Protein Secretion. Trends Cell Biol. 2017 Mar;27(3):230–40.
13. Pallotta MT, Nickel W. FGF2 and IL-1β - explorers of unconventional secretory pathways at a glance. J Cell Sci [Internet]. 2020 Nov;133(21). Available from: https://pubmed.ncbi.nlm.nih.gov/33154173/
14. Zhang M, Kenny SJ, Ge L, Xu K, Schekman R. Translocation of interleukin-1β into a vesicle intermediate in autophagy-mediated secretion. eLife. 2015 Nov 2;4:e11205.
15. Villeneuve J, Bassaganyas L, Lepreux S, Chiritoiu M, Costet P, Ripoche J, et al. Unconventional secretion of FABP4 by endosomes and secretory lysosomes. J Cell Biol. 2018 Feb 5;217(2):649–65.
16. Dupont N, Jiang S, Pilli M, Ornatowski W, Bhattacharya D, Deretic V. Autophagy-based unconventional secretory pathway for extracellular delivery of IL-1β. EMBO J. 2011 Nov;30(23):4701–11.
17. Lee JG, Takahama S, Zhang G, Tomarev SI, Ye Y. Unconventional secretion of misfolded proteins promotes adaptation to proteasome dysfunction in mammalian cells. Nat Cell Biol. 2016;
18. Liu DA, Tao K, Wu B, Yu Z, Szczepaniak M, Rames M, et al. A phosphoinositide switch mediates exocyst recruitment to multivesicular endosomes for exosome secretion. Nat Commun. 2023 Oct 28;14(1):6883.
19. Buratta S, Tancini B, Sagini K, Delo F, Chiaradia E, Urbanelli L, et al. Lysosomal Exocytosis, Exosome Release and Secretory Autophagy: The Autophagic- and Endo-Lysosomal Systems Go Extracellular. Int J Mol Sci. 2020;
20. Bruns C, McCaffery JM, Curwin AJ, Duran JM, Malhotra V. Biogenesis of a novel compartment for autophagosome-mediated unconventional protein secretion. J Cell Biol. 2011 Dec 12;195(6):979–92.
21. Cruz-Garcia D, Curwin AJ, Popoff JF, Bruns C, Duran JM, Malhotra V. Remodeling of secretory compartments creates CUPS during nutrient starvation. J Cell Biol. 2014 Dec 22;207(6):695–703.
22. Cruz-Garcia D, Brouwers N, Duran JM, Mora G, Curwin AJ, Malhotra V. A diacidic motif determines unconventional secretion of wild-type and ALS-linked mutant SOD1. J Cell Biol. 2017 Sep;216(9):2691–700.
23. Cruz-Garcia D, Brouwers N, Malhotra V, Curwin AJ. Reactive oxygen species triggers

874 unconventional secretion of antioxidants and Acb1. J Cell Biol. 2020 Apr 6;219(4):e201905028.
875 24. Gee HY, Noh SH, Tang BL, Kim KH, Lee MG. Rescue of ΔF508-CFTR trafficking via a
876 GRASP-dependent unconventional secretion pathway. Cell. 2011 Sep;146(5):746–60.
877 25. Gee HY, Kim J, Lee MG. Unconventional secretion of transmembrane proteins. Semin Cell Dev
878 Biol. 2018 Nov;83:59–66.
879 26. Meldolesi J. Unconventional Protein Secretion Dependent on Two Extracellular Vesicles:
880 Exosomes and Ectosomes. Front Cell Dev Biol. 2022;10:877344.
881 27. Senol AD, Samarani M, Syan S, Guardia CM, Nonaka T, Liv N, et al. α-Synuclein fibrils subvert
882 lysosome structure and function for the propagation of protein misfolding between cells through
883 tunneling nanotubes. PLoS Biol [Internet]. 2021 Jul;19(7). Available from:
884 https://pubmed.ncbi.nlm.nih.gov/34283825/
885 28. Abounit S, Wu JW, Duff K, Victoria GS, Zurzolo C. Tunneling nanotubes: A possible highway
886 in the spreading of tau and other prion-like proteins in neurodegenerative diseases. Prion. 2016
887 Sep;10(5):344–51.
888 29. Zurzolo C. Tunneling nanotubes: Reshaping connectivity. Curr Opin Cell Biol. 2021
889 Aug;71:139–47.
890 30. Chiritoiu M, Brouwers N, Turacchio G, Pirozzi M, Malhotra V. GRASP55 and UPR Control
891 Interleukin-1β Aggregation and Secretion. Dev Cell. 2019 Apr 8;49(1):145-155.e4.
892 31. Gee HY, Noh SH, Tang BL, Kim KH, Lee MG. Rescue of ΔF508-CFTR trafficking via a
893 GRASP-dependent unconventional secretion pathway. Cell. 2011 Sep 2;146(5):746–60.
894 32. Zhang X, Wang L, Ireland SC, Ahat E, Li J, Bekier ME, et al. GORASP2/GRASP55
895 collaborates with the PtdIns3K UVRAG complex to facilitate autophagosome-lysosome fusion.
896 Autophagy. 2019;15(10):1787–800.
897 33. Nüchel J, Tauber M, Nolte JL, Mörgelin M, Türk C, Eckes B, et al. An mTORC1-GRASP55
898 signaling axis controls unconventional secretion to reshape the extracellular proteome upon stress. Mol
899 Cell. 2021 Aug 19;81(16):3275-3293.e12.
900 34. Tancini B, Buratta S, Delo F, Sagini K, Chiaradia E, Pellegrino RM, et al. Lysosomal
901 Exocytosis: The Extracellular Role of an Intracellular Organelle. Membranes. 2020 Dec 9;10(12):406.
902 35. Ghosh S, Dellibovi-Ragheb TA, Kerviel A, Pak E, Qiu Q, Fisher M, et al. β-Coronaviruses Use
903 Lysosomes for Egress Instead of the Biosynthetic Secretory Pathway. Cell. 2020 Dec 10;183(6):1520-
904 1535.e14.
905 36. Xu Y, Du S, Marsh JA, Horie K, Sato C, Ballabio A, et al. TFEB regulates lysosomal exocytosis
906 of tau and its loss of function exacerbates tau pathology and spreading. Mol Psychiatry [Internet]. 2020;
907 Available from: https://pubmed.ncbi.nlm.nih.gov/32366951/
908 37. Medina DL, Fraldi A, Bouche V, Annunziata F, Mansueto G, Spampanato C, et al.
909 Transcriptional activation of lysosomal exocytosis promotes cellular clearance. Dev Cell. 2011 Sep
910 13;21(3):421–30.
911 38. Abounit S, Bousset L, Loria F, Zhu S, de Chaumont F, Pieri L, et al. Tunneling nanotubes spread
912 fibrillar α-synuclein by intercellular trafficking of lysosomes. EMBO J. 2016 Oct 4;35(19):2120–38.
913 39. Cao H, Sekiya M, Ertunc ME, Burak MF, Mayers JR, White A, et al. Adipocyte lipid chaperone
914 aP2 Is a secreted adipokine regulating hepatic glucose production. Cell Metab. 2013;
915 40. Evavold CL, Ruan J, Tan Y, Xia S, Wu H, Kagan JC. The Pore-Forming Protein Gasdermin D
916 Regulates Interleukin-1 Secretion from Living Macrophages. Immunity. 2018;
917 41. Fourriere L, Divoux S, Roceri M, Perez F, Boncompain G. Microtubule-independent secretion
918 requires functional maturation of Golgi elements. J Cell Sci. 2016 Sep 1;129(17):3238–50.
919 42. Steringer JP, Lange S, Čujová S, Šachl R, Poojari C, Lolicato F, et al. Key steps in
920 unconventional secretion of fibroblast growth factor 2 reconstituted with purified components. eLife.
921 2017 Jul;6.
922 43. Evavold CL, Ruan J, Tan Y, Xia S, Wu H, Kagan JC. The Pore-Forming Protein Gasdermin D
923 Regulates Interleukin-1 Secretion from Living Macrophages. Immunity. 2018 Jan 16;48(1):35-44.e6.
924 44. Sitia R, Rubartelli A. The unconventional secretion of IL-1β: Handling a dangerous weapon to
925 optimize inflammatory responses. Semin Cell Dev Biol. 2018 Nov;83:12–21.
926 45. Popa SJ, Stewart SE, Moreau K. Unconventional secretion of annexins and galectins. Semin
927 Cell Dev Biol. 2018 Nov;83:42–50.
928 46. Wu S, Hernandez Villegas NC, Sirkis DW, Thomas-Wright I, Wade-Martins R, Schekman R.

Unconventional secretion of α-synuclein mediated by palmitoylated DNAJC5 oligomers. eLife. 2023 Jan 10;12:e85837.
47. Gosset P, Camu W, Raoul C, Mezghrani A. Prionoids in amyotrophic lateral sclerosis. Brain Commun. 2022;4(3):fcac145.
48. Katsinelos T, Zeitler M, Dimou E, Karakatsani A, Müller HM, Nachman E, et al. Unconventional Secretion Mediates the Trans-cellular Spreading of Tau. Cell Rep. 2018 May;23(7):2039–55.
49. Katsinelos T, McEwan WA, Jahn TR, Nickel W. Identification of cis-acting determinants mediating the unconventional secretion of tau. Sci Rep. 2021 Dec;11(1).
50. Azad T, Tashakor A, Hosseinkhani S. Split-luciferase complementary assay: applications, recent developments, and future perspectives. Anal Bioanal Chem. 2014 Sep;406(23):5541–60.
51. Boncompain G, Divoux S, Gareil N, De Forges H, Lescure A, Latreche L, et al. Synchronization of secretory protein traffic in populations of cells. Nat Methods. 2012;
52. Misumi Y, Misumi Y, Miki K, Takatsuki A, Tamura G, Ikehara Y. Novel blockade by brefeldin A of intracellular transport of secretory proteins in cultured rat hepatocytes. J Biol Chem. 1986;
53. Lippincott-Schwartz J, Yuan LC, Bonifacino JS, Klausner RD. Rapid redistribution of Golgi proteins into the ER in cells treated with brefeldin A: evidence for membrane cycling from Golgi to ER. Cell. 1989 Mar 10;56(5):801–13.
54. Mardones GA, Snyder CM, Howell KE. Cis-Golgi matrix proteins move directly to endoplasmic reticulum exit sites by association with tubules. Mol Biol Cell. 2006 Jan;17(1):525–38.
55. Carr CM, Rizo J. At the junction of SNARE and SM protein function. Curr Opin Cell Biol. 2010;
56. Brunello CA, Merezhko M, Uronen RL, Huttunen HJ. Mechanisms of secretion and spreading of pathological tau protein. Cell Mol Life Sci CMLS. 2020 May;77(9):1721–44.
57. Zhang M, Liu L, Lin X, Wang Y, Li Y, Guo Q, et al. A Translocation Pathway for Vesicle-Mediated Unconventional Protein Secretion. Cell. 2020 Apr 30;181(3):637-652.e15.
58. Liu L, Zhang M, Ge L. Protein translocation into the ERGIC: an upstream event of secretory autophagy. Autophagy. 2020 Jul;16(7):1358–60.
59. Sun Y, Tao X, Han Y, Lin X, Tian R, Wang H, et al. A dual role of ERGIC-localized Rabs in TMED10-mediated unconventional protein secretion. Nat Cell Biol. 2024 Jul;26(7):1077–92.
60. Munro S, Pelham HR. A C-terminal signal prevents secretion of luminal ER proteins. Cell. 1987 Mar 13;48(5):899–907.
61. Lewis MJ, Pelham HR. Ligand-induced redistribution of a human KDEL receptor from the Golgi complex to the endoplasmic reticulum. Cell. 1992 Jan 24;68(2):353–64.
62. Byström R, Andersen PM, Gröbner G, Oliveberg M. SOD1 mutations targeting surface hydrogen bonds promote amyotrophic lateral sclerosis without reducing apo-state stability. J Biol Chem. 2010 Jun 18;285(25):19544–52.
63. Khurana V, Lu Y, Steinhilb ML, Oldham S, Shulman JM, Feany MB. TOR-Mediated Cell-Cycle Activation Causes Neurodegeneration in a Drosophila Tauopathy Model. Curr Biol. 2006 Feb 7;16(3):230–41.
64. Bramblett GT, Goedert M, Jakes R, Merrick SE, Trojanowski JQ, Lee VM. Abnormal tau phosphorylation at Ser396 in Alzheimer's disease recapitulates development and contributes to reduced microtubule binding. Neuron. 1993 Jun;10(6):1089–99.
65. Talmat-Amar Y, Arribat Y, Redt-Clouet C, Feuillette S, Bougé AL, Lecourtois M, et al. Important neuronal toxicity of microtubule-bound Tau in vivo in Drosophila. Hum Mol Genet. 2011 Oct 1;20(19):3738–45.
66. Grundke-Iqbal I, Iqbal K, Tung YC, Quinlan M, Wisniewski HM, Binder LI. Abnormal phosphorylation of the microtubule-associated protein tau (tau) in Alzheimer cytoskeletal pathology. Proc Natl Acad Sci. 1986 Jul;83(13):4913–7.
67. Lopez DM, Maltby CJ, Warming H, Divecha N, Vargas-Caballero M, Coldwell MJ, et al. A luminescence-based reporter to study tau secretion reveals overlapping mechanisms for the release of healthy and pathological tau. Front Neurosci. 2023;17:1196007.
68. Barthélemy NR, Saef B, Li Y, Gordon BA, He Y, Horie K, et al. CSF tau phosphorylation occupancies at T217 and T205 represent improved biomarkers of amyloid and tau pathology in Alzheimer's disease. Nat Aging. 2023 Apr;3(4):391–401.

69. Sperfeld AD, Collatz MB, Baier H, Palmbach M, Storch A, Schwarz J, et al. FTDP-17: an early-onset phenotype with parkinsonism and epileptic seizures caused by a novel mutation. Ann Neurol. 1999 Nov;46(5):708–15.
70. Goedert M, Jakes R, Crowther RA. Effects of frontotemporal dementia FTDP-17 mutations on heparin-induced assembly of tau filaments. FEBS Lett. 1999 May 7;450(3):306–11.
71. Cotman CW, Poon WW, Rissman RA, Blurton-Jones M. The role of caspase cleavage of tau in Alzheimer disease neuropathology. J Neuropathol Exp Neurol. 2005 Feb;64(2):104–12.
72. Guillozet-Bongaarts AL, Garcia-Sierra F, Reynolds MR, Horowitz PM, Fu Y, Wang T, et al. Tau truncation during neurofibrillary tangle evolution in Alzheimer's disease. Neurobiol Aging. 2005 Jul;26(7):1015–22.
73. Guillozet-Bongaarts AL, Cahill ME, Cryns VL, Reynolds MR, Berry RW, Binder LI. Pseudophosphorylation of tau at serine 422 inhibits caspase cleavage: in vitro evidence and implications for tangle formation in vivo. J Neurochem. 2006 May;97(4):1005–14.
74. Bellenguez C, Küçükali F, Jansen IE, Kleineidam L, Moreno-Grau S, Amin N, et al. New insights into the genetic etiology of Alzheimer's disease and related dementias. Nat Genet. 2022 Apr;54(4):412–36.
75. Satoh K, Abe-Dohmae S, Yokoyama S, St George-Hyslop P, Fraser PE. ATP-binding cassette transporter A7 (ABCA7) loss of function alters Alzheimer amyloid processing. J Biol Chem. 2015 Oct 2;290(40):24152–65.
76. Bhattacharyya R, Teves CAF, Long A, Hofert M, Tanzi RE. The neuronal-specific isoform of BIN1 regulates β-secretase cleavage of APP and Aβ generation in a RIN3-dependent manner. Sci Rep. 2022 Mar 3;12:3486.
77. Andersen OM, Reiche J, Schmidt V, Gotthardt M, Spoelgen R, Behlke J, et al. Neuronal sorting protein-related receptor sorLA/LR11 regulates processing of the amyloid precursor protein. Proc Natl Acad Sci U S A. 2005 Sep 20;102(38):13461–6.
78. Wolfe MS, Xia W, Ostaszewski BL, Diehl TS, Kimberly WT, Selkoe DJ. Two transmembrane aspartates in presenilin-1 required for presenilin endoproteolysis and gamma-secretase activity. Nature. 1999 Apr 8;398(6727):513–7.
79. Seegar TCM, Killingsworth LB, Saha N, Meyer PA, Patra D, Zimmerman B, et al. Structural Basis for Regulated Proteolysis by the α-Secretase ADAM10. Cell. 2017 Dec 14;171(7):1638-1648.e7.
80. Q X, Sc G, P Y, Y W, S H, E G, et al. Role of phosphatidylinositol clathrin assembly lymphoid-myeloid leukemia (PICALM) in intracellular amyloid precursor protein (APP) processing and amyloid plaque pathogenesis. J Biol Chem [Internet]. 2012 Jun 15 [cited 2024 Oct 6];287(25). Available from: https://pubmed.ncbi.nlm.nih.gov/22539346/
81. Eysert F, Coulon A, Boscher E, Vreulx AC, Flaig A, Mendes T, et al. Alzheimer's genetic risk factor FERMT2 (Kindlin-2) controls axonal growth and synaptic plasticity in an APP-dependent manner. Mol Psychiatry. 2021 Oct;26(10):5592–607.
82. Kim S, Chun H, Kim Y, Kim Y, Park U, Chu J, et al. Astrocytic autophagy plasticity modulates Aβ clearance and cognitive function in Alzheimer's disease. Mol Neurodegener. 2024 Jul 23;19(1):55.
83. Eccles MK, Main N, Carlessi R, Armstrong AM, Sabale M, Roberts-Mok B, et al. Quantitative comparison of presenilin protein expression reveals greater activity of PS2-γ-secretase. FASEB J Off Publ Fed Am Soc Exp Biol. 2024 Jan;38(1):e23396.
84. Li Y, Liu D, Zhang X, Rimal S, Lu B, Li S. RACK1 and IRE1 participate in the translational quality control of amyloid precursor protein in Drosophila models of Alzheimer's disease. J Biol Chem. 2024 Feb 2;300(3):105719.
85. J H, Dj S. The amyloid hypothesis of Alzheimer's disease: progress and problems on the road to therapeutics. Science [Internet]. 2002 Jul 19 [cited 2024 Oct 6];297(5580). Available from: https://pubmed.ncbi.nlm.nih.gov/12130773/
86. Nixon RA, Rubinsztein DC. Mechanisms of autophagy-lysosome dysfunction in neurodegenerative diseases. Nat Rev Mol Cell Biol. 2024 Nov;25(11):926–46.
87. Annunziata I, Patterson A, Helton D, Hu H, Moshiach S, Gomero E, et al. Lysosomal NEU1 deficiency affects amyloid precursor protein levels and amyloid-β secretion via deregulated lysosomal exocytosis. Nat Commun. 2013;4:2734.
88. Masters CL, Beyreuther K. Alzheimer's centennial legacy: prospects for rational therapeutic intervention targeting the Abeta amyloid pathway. Brain J Neurol. 2006 Nov;129(Pt 11):2823–39.

89. Cruz-Garcia D, Malhotra V, Curwin AJ. Unconventional protein secretion triggered by nutrient starvation. Semin Cell Dev Biol. 2018;
90. Wang Y, Huang M, Mu X, Song W, Guo Q, Zhang M, et al. TMED10-mediated unconventional secretion of IL-33 regulates intestinal epithelium differentiation and homeostasis. Cell Res. 2024 Mar;34(3):258–61.
91. Goedert M, Masuda-Suzukake M, Falcon B. Like prions: the propagation of aggregated tau and α-synuclein in neurodegeneration. Brain J Neurol. 2017 Feb;140(2):266–78.
92. Mudher A, Colin M, Dujardin S, Medina M, Dewachter I, Alavi Naini SM, et al. What is the evidence that tau pathology spreads through prion-like propagation? Acta Neuropathol Commun. 2017 Dec 19;5(1):99.
93. Padmanabhan S, Biswal MR, Manjithaya R, Prakash MK. Exploring the context of diacidic motif DE as a signal for unconventional protein secretion in eukaryotic proteins. Wellcome Open Res. 2018;3:148.
94. Semino C, Carta S, Gattorno M, Sitia R, Rubartelli A. Progressive waves of IL-1β release by primary human monocytes via sequential activation of vesicular and gasdermin D-mediated secretory pathways. Cell Death Dis. 2018 Oct 23;9(11):1088.
95. Long JM, Holtzman DM. Alzheimer Disease: An Update on Pathobiology and Treatment Strategies. Cell. 2019 Oct 3;179(2):312–39.
96. Tanaka Y, Yamada K, Satake K, Nishida I, Heuberger M, Kuwahara T, et al. Seeding Activity-Based Detection Uncovers the Different Release Mechanisms of Seed-Competent Tau Versus Inert Tau via Lysosomal Exocytosis. Front Neurosci. 2019;13:1258.
97. Ahat E, Bui S, Zhang J, da Veiga Leprevost F, Sharkey L, Reid W, et al. GRASP55 regulates the unconventional secretion and aggregation of mutant huntingtin. J Biol Chem. 2022 Aug;298(8):102219.
98. Bae EJ, Choi M, Kim JT, Kim DK, Jung MK, Kim C, et al. TNF-α promotes α-synuclein propagation through stimulation of senescence-associated lysosomal exocytosis. Exp Mol Med. 2022 Jun;54(6):788–800.
99. Xie YX, Naseri NN, Fels J, Kharel P, Na Y, Lane D, et al. Lysosomal exocytosis releases pathogenic α-synuclein species from neurons in synucleinopathy models. Nat Commun. 2022 Aug 22;13(1):4918.
100. Zhao X, Guan Y, Liu F, Yan S, Wang Y, Hu M, et al. SNARE Proteins Mediate α-Synuclein Secretion via Multiple Vesicular Pathways. Mol Neurobiol. 2022 Jan;59(1):405–19.
101. Lopez A, Siddiqi FH, Villeneuve J, Ureshino RP, Jeon HY, Koulousakis P, et al. Carbonic anhydrase inhibition ameliorates tau toxicity via enhanced tau secretion. Nat Chem Biol. 2024 Oct 31;

Figure 1 :

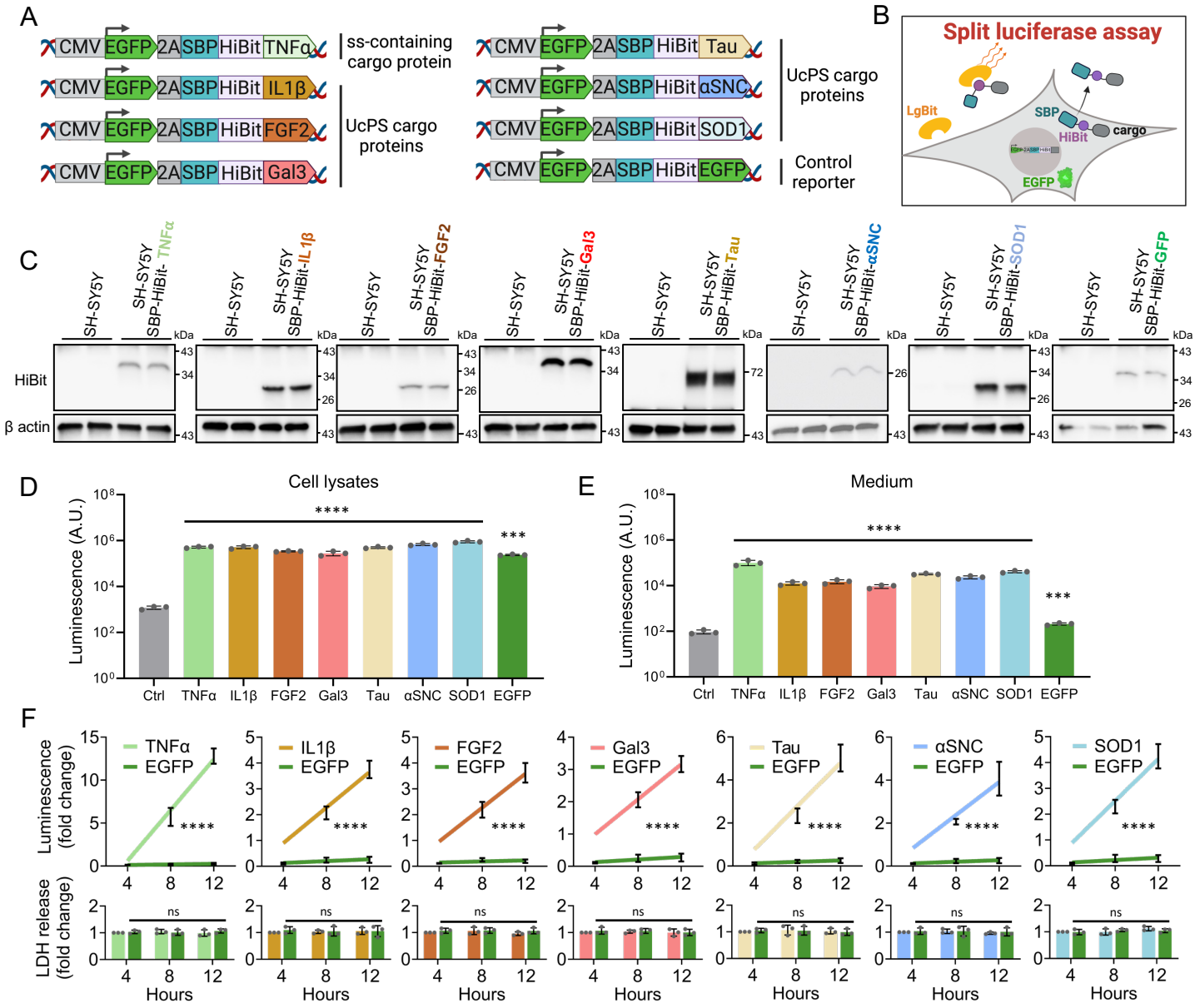
A
CMV EGFP 2A SBP HiBit TNFα
CMV EGFP 2A SBP HiBit IL1β
CMV EGFP 2A SBP HiBit FGF2
CMV EGFP 2A SBP HiBit Gal3
ss-containing cargo protein
UcPS cargo proteins
CMV EGFP 2A SBP HiBit Tau
CMV EGFP 2A SBP HiBit αSNC
CMV EGFP 2A SBP HiBit SOD1
CMV EGFP 2A SBP HiBit EGFP
UcPS cargo proteins
Control reporter
B
Split luciferase assay
LgBit
SBP
HiBit
cargo
EGFP
C
SH-SY5Y
SH-SY5Y SBP-HiBit-TNFα
SH-SY5Y SBP-HiBit-IL1β
SH-SY5Y SBP-HiBit-FGF2
SH-SY5Y SBP-HiBit-Gal3
SH-SY5Y SBP-HiBit-Tau
SH-SY5Y SBP-HiBit-αSNC
SH-SY5Y SBP-HiBit-SOD1
SH-SY5Y SBP-HiBit-GFP
kDa
HiBit
β actin
D
Cell lysates
Luminescence (A.U.)
Ctrl TNFα IL1β FGF2 Gal3 Tau αSNC SOD1 EGFP
E
Medium
F
Luminescence (fold change)
LDH release (fold change)
TNFα EGFP
IL1β EGFP
FGF2 EGFP
Gal3 EGFP
Tau EGFP
αSNC EGFP
SOD1 EGFP
ns
Hours

Figure 2 :

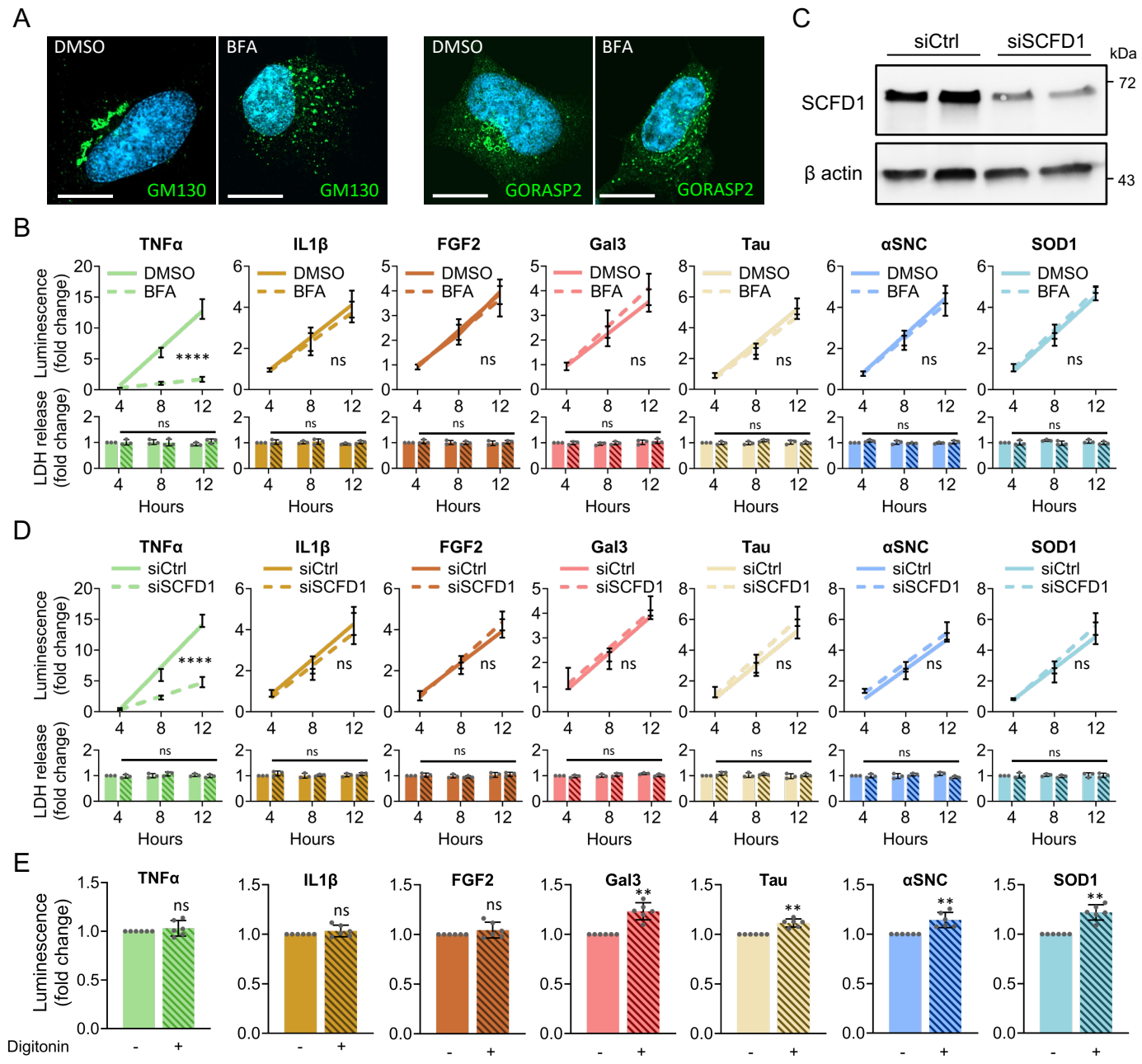
A
DMSO
BFA
GM130
GORASP2
C
siCtrl
siSCFD1
kDa
SCFD1
β actin
72
43
B
TNFα
IL1β
FGF2
Gal3
Tau
αSNC
SOD1
DMSO
BFA
Luminescence (fold change)
LDH release (fold change)
****
ns
Hours
D
siCtrl
siSCFD1
E
Digitonin
**

Figure 3 :

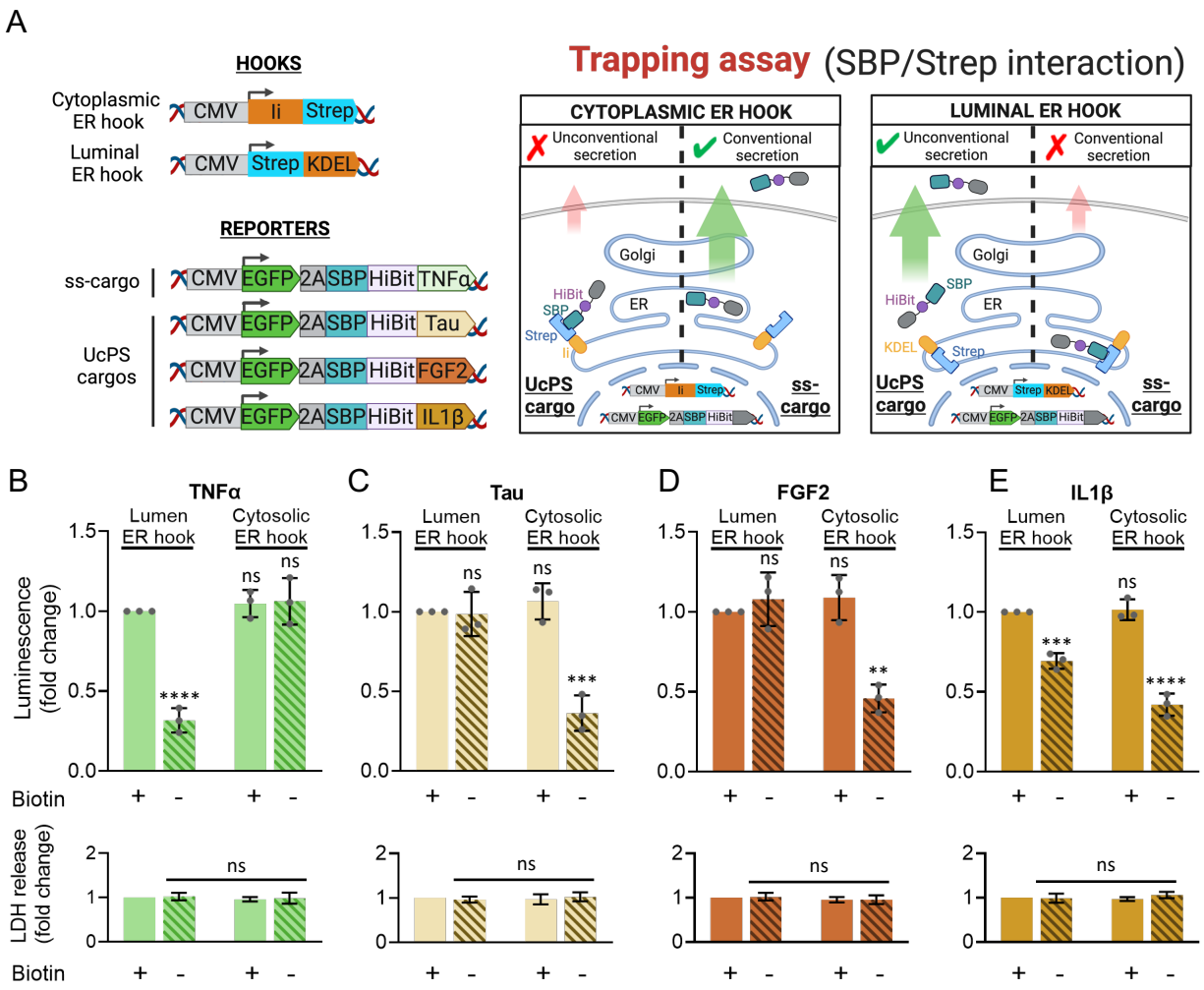
A
HOOKS
Cytoplasmic ER hook
CMV Ii Strep
Luminal ER hook
CMV Strep KDEL
REPORTERS
ss-cargo
CMV EGFP 2A SBP HiBit TNFα
UcPS cargos
CMV EGFP 2A SBP HiBit Tau
CMV EGFP 2A SBP HiBit FGF2
CMV EGFP 2A SBP HiBit IL1β
Trapping assay (SBP/Strep interaction)
CYTOPLASMIC ER HOOK
Unconventional secretion
Conventional secretion
Golgi
ER
HiBit
SBP
Strep
Ii
UcPS cargo
ss-cargo
LUMINAL ER HOOK
Unconventional secretion
Conventional secretion
Golgi
ER
HiBit
SBP
KDEL
Strep
UcPS cargo
ss-cargo
B
TNFα
C
Tau
D
FGF2
E
IL1β
Lumen ER hook
Cytosolic ER hook
Luminescence (fold change)
LDH release (fold change)
Biotin
ns
****
***
**

Figure 4 :

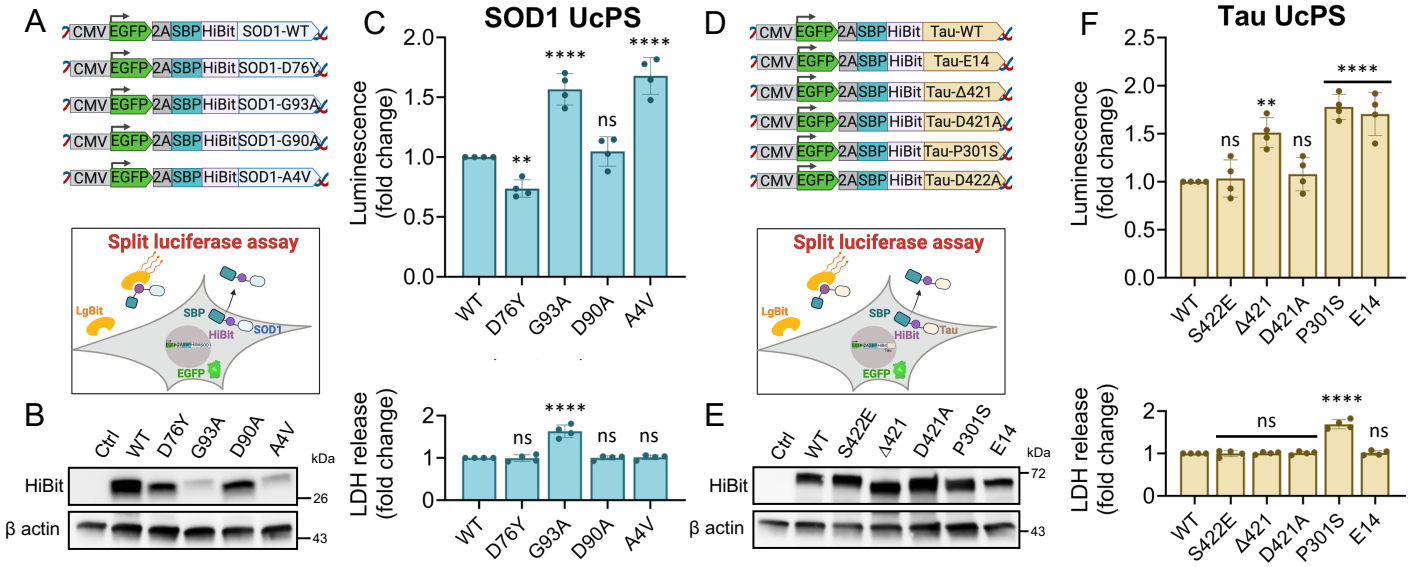
A
CMV EGFP 2A SBP HiBit SOD1-WT
CMV EGFP 2A SBP HiBit SOD1-D76Y
CMV EGFP 2A SBP HiBit SOD1-G93A
CMV EGFP 2A SBP HiBit SOD1-G90A
CMV EGFP 2A SBP HiBit SOD1-A4V
Split luciferase assay
LgBit
SBP
HiBit
SOD1
EGFP
B
Ctrl
WT
D76Y
G93A
D90A
A4V
kDa
HiBit
β actin
26
43
C
SOD1 UcPS
Luminescence (fold change)
2.0
1.5
1.0
0.5
0.0
**
****
ns
****
WT
D76Y
G93A
D90A
A4V
LDH release (fold change)
2
1
0
ns
****
ns
ns
D
CMV EGFP 2A SBP HiBit Tau-WT
CMV EGFP 2A SBP HiBit Tau-E14
CMV EGFP 2A SBP HiBit Tau-Δ421
CMV EGFP 2A SBP HiBit Tau-D421A
CMV EGFP 2A SBP HiBit Tau-P301S
CMV EGFP 2A SBP HiBit Tau-D422A
Split luciferase assay
LgBit
SBP
HiBit
Tau
EGFP
E
Ctrl
WT
S422E
Δ421
D421A
P301S
E14
kDa
HiBit
β actin
72
43
F
Tau UcPS
Luminescence (fold change)
2.5
2.0
1.5
1.0
0.5
0.0
ns
**
ns
****
WT
S422E
Δ421
D421A
P301S
E14
LDH release (fold change)
2
1
0
ns
****
ns

Figure 5 :

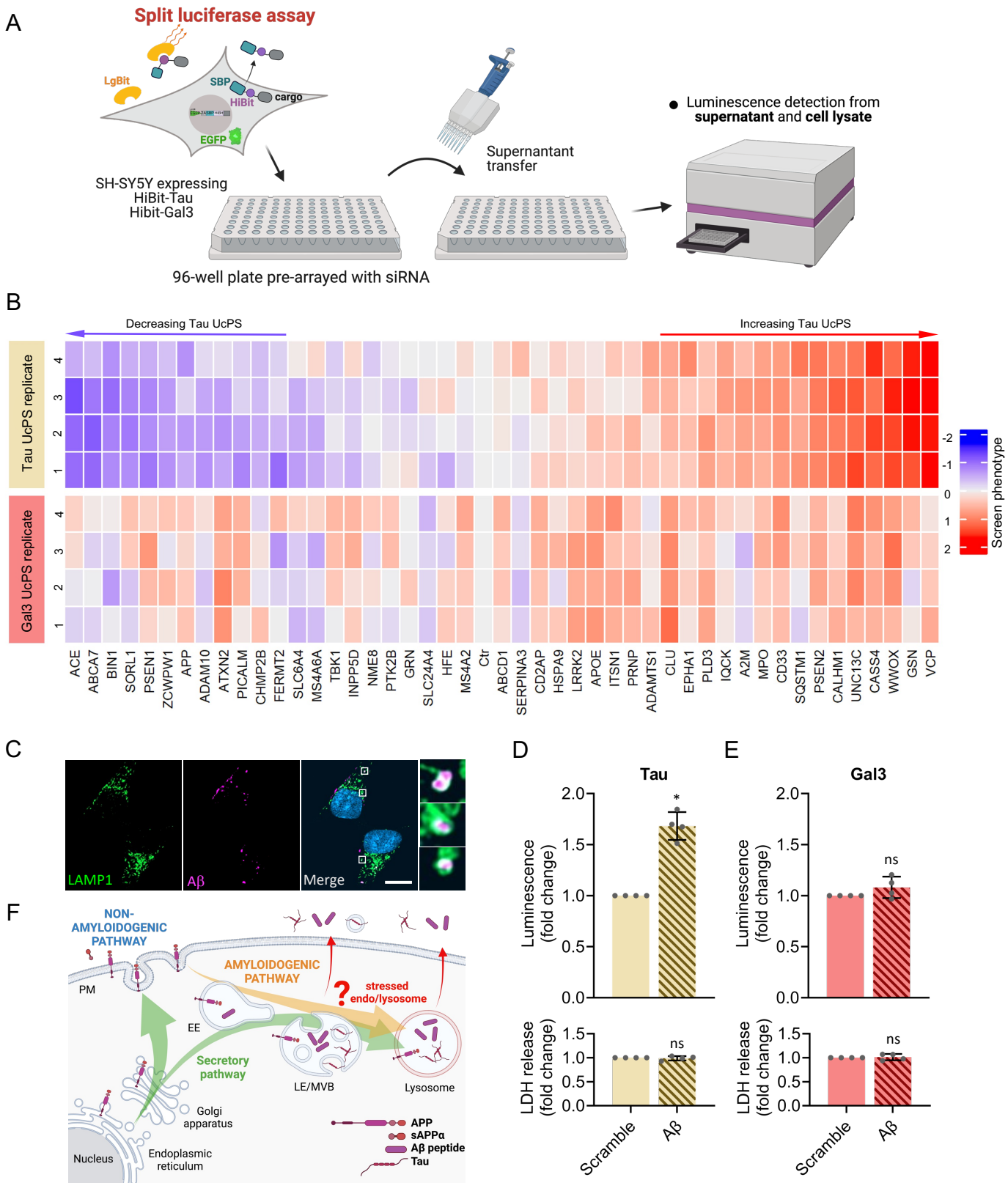
A
Split luciferase assay
LgBit
SBP
HiBit
cargo
EGFP
SH-SY5Y expressing
HiBit-Tau
Hibit-Gal3
96-well plate pre-arrayed with siRNA
Supernantant
transfer
Luminescence detection from
supernatant and cell lysate
B
Decreasing Tau UcPS
Increasing Tau UcPS
Tau UcPS replicate
Gal3 UcPS replicate
Screen phenotype
ACE ABCA7 BIN1 SORL1 PSEN1 ZCWPW1 APP ADAM10 ATXN2 PICALM CHMP2B FERMT2 SLC6A4 MS4A6A TBK1 INPP5D NME8 PTK2B GRN SLC24A4 HFE MS4A2 Ctr ABCD1 SERPINA3 CD2AP HSPA9 LRRK2 APOE ITSN1 PRNP ADAMTS1 CLU EPHA1 PLD3 IQCK A2M MPO CD33 SQSTM1 PSEN2 CALHM1 UNC13C CASS4 WWOX GSN VCP
C
LAMP1
Aβ
Merge
D
Tau
Luminescence (fold change)
LDH release (fold change)
Scramble
Aβ
E
Gal3
ns
F
NON-AMYLOIDOGENIC PATHWAY
AMYLOIDOGENIC PATHWAY
stressed endo/lysosome
PM
EE
Secretory pathway
LE/MVB
Lysosome
Golgi apparatus
Nucleus
Endoplasmic reticulum
APP
sAPPα
Aβ peptide
Tau